Kinesin-1-mediated capsid disassembly and disruption of the nuclear pore complex promote virus infection

Strunze, S ; Engelke, M F ; Wang, I-H ; Puntener, D ; Boucke, K ; Schleich, S ; Way, M ; Schoenenberger, P ; Burckhardt, C J ; Greber, U F

Abstract: Many viruses deliver their genomes into the host cell nucleus for replication. However, the size restrictions of the nuclear pore complex (NPC), which regulates the passage of proteins, nucleic acids, and solutes through the nuclear envelope, require virus capsid uncoating before viral DNA can access the nucleus. We report a microtubule motor kinesin-1-mediated and NPC-supported mechanism of adenovirus uncoating. The capsid binds to the NPC filament protein Nup214 and kinesin-1 light-chain Klc1/2. The nucleoporin Nup358, which is bound to Nup214/Nup88, interacts with the kinesin-1 heavy-chain Kif5c to indirectly link the capsid to the kinesin motor. Kinesin-1 disrupts capsids docked at Nup214, which compromises the NPC and dislocates nucleoporins and capsid fragments into the cytoplasm. NPC disruption increases nuclear envelope permeability as indicated by the nuclear influx of large cytoplasmic dextran polymers. Thus, kinesin-1 uncoats viral DNA and compromises NPC integrity, allowing viral genomes nuclear access to promote infection.

DOI: https://doi.org/10.1016/j.chom.2011.08.010

Kinesin-1 mediated capsid disassembly and disruption of the nuclear pore complex promote virus infection

Sten Strunze[§1], Martin F. Engelke[§1], I-Hsuan Wang[§], Daniel Puntener[§], Karin Boucke[§], Sibylle Schleich[†], Michael Way[†], Philipp Schoenenberger[§], Christoph J. Burckhardt[§Y] & Urs F. Greber[§+]

§ University of Zürich, Institute of Molecular Life Sciences,

Winterthurerstrasse 190, CH-8057 Zürich, Switzerland

1 equal contribution

† Cancer Research UK, Lincoln's Inn Field, London, UK

y Present address: Department of Cell Biology, Harvard Medical School,

Boston, Massachusetts 02115, USA

+ corresponding author:

Telephone: +41 446354841 Fax: +41 446356817

Email: urs.greber@imls.uzh.ch

Keywords: kinesin; DNA tumor virus; nuclear pore complex; Nup214; Nup358; nuclear import; virus uncoating; disassembly; microtubule; motor protein; DNA import; nuclear transport; heavy chain; light chain; protein IX;

Short title: Kinesin disrupts virus and nuclear pore complex

Abstract

The nuclear pore complex (NPC) allows passage of proteins, nucleic acids and solutes through the nuclear envelope. Viruses use the NPC to deliver their genomes into the nucleus. Here we report that NPCs supports the uncoating of adenovirus by the microtubule motor kinesin-1 Kif5C. Kinesin-1 light chain binds the capsid protein IX and links the virus to Kif5C, which is also bound to and activated by the NPC filament protein Nup358. Kinesin-1 breaks open capsids docked at the nucleoporin Nup214. This process disrupts the NPC, as nucleoporins are dislocated from the NPC to the cytoplasm together with capsid fragments. NPC disruption increases the permeability of the nuclear envelope indicated by influx of large dextran polymers from the cytoplasm into the nucleus. Our data show that kinesin-1 uncoats the viral DNA at the NPC, and compromises the integrity of the NPC, thus allowing viral genome access to the nucleus and infection.

Introduction

In eukaryotic cells transport between the nucleus and the cytoplasm during interphase is controlled by the nuclear pore complex (NPC). The NPC is a supra-molecular assembly of at least 30 different proteins (Alber et al., 2007; D'Angelo and Hetzer, 2008). It is anchored in the nuclear envelope by several transmembrane nucleoporins (Nups). Membrane-proximal scaffolding Nups maintain the framework of the NPC, while central and peripheral phenylalanine-glycine (FxFG and GLFG) rich Nups provide a selective phase barrier, which controls passive diffusion and facilitated transport of macromolecules through the NPC. The NPC has barrier and transport functions, with cargo size restriction of about 39 nm for receptor-mediated transport and solutes of about 40 kD (Mohr et al., 2009; Pante and Kann, 2002). FG-repeat containing peripheral Nups including Nup358 (also referred to as RanBP2) and Nup153 are predicted to form a non-cohesive dynamic network based on a higher fraction of charged amino acid residues between FG domains compared to the cohesive Nups, and thereby act as an entropic barrier (Lim et al., 2007; Patel et al., 2007; Ribbeck and Gorlich, 2002). Proteins and nucleic acids bound to import or export receptors are transported through the NPC by a facilitated mechanism involving cumulative reversible steps on natively unfolded FxFG and GLFG rich Nups and a final irreversible exit step (Frey and Gorlich, 2007; Lowe et al., 2010; Patel et al., 2007).

NPCs of mammalian cells are largely immobile, but their peripheral proteins can have short residence times of seconds to minutes, suggesting that NPC substructures are highly dynamic and may have multiple functions (Daigle et al., 2001). For example, NPCs dynamically interact with chromatin thereby controlling genome organization and gene expression. They also recruit motor proteins, such as dynein-dynactin, which binds to Nup358 of the cytoplasmic NPC filaments in the

G2 phase of the cell cycle (Splinter et al., 2010), or kinesin-1 throughout interphase (Cai et al., 2001). NPC malfunction or mutations in nucleoporins have been associated with human pathologies, including cancer and cardiac diseases (Zhang et al., 2008). As we age, NPCs also become leaky due to oxidative damage and proteasome-mediated degradation of the stable NPC-resident scaffolding Nups (D'Angelo et al., 2009).

The size restriction of normal NPCs precludes most viral capsids from directly accessing the nucleus (reviewed in Puntener and Greber, 2009; Suzuki and Craigie, 2007). Yet certain viruses deliver their genome into the nucleus, and uncoat in the cytoplasm. Nuclear import of reverse transcribed HIV pre-integration complex, for example, is restricted by cellular factors binding to the viral capsid, and depends on Nups, in particular the FG-containing Nup153 (Lee et al., 2010; Woodward et al., 2009). Herpesviruses dock to the NPC predominantly by Nup214 (Copeland et al., 2009; Pasdeloup et al., 2009), and are thought to import DNA using a pressure-based mechanism (Newcomb et al., 2001; Rao and Feiss, 2008). Adenoviruses are also critically dependent on nuclear import of their genome. They cause respiratory, gastrointestinal, urogenital and ocular disease with epidemic potential and occasionally fatal outcomes (Hayashi and Hogg, 2007; Kojaoghlanian et al., 2003). Humand adenovirus type 2/5 (HAdV-2/5, short Ad2/5) enters polarized epithelial cells by triggering a cytokine response from macrophages, which leads to relocation of the coxsackievirus Ad receptor CAR and integrin co-receptors to the apical plasma membrane (Lutschg et al., 2011). The virus subsequently exposes the viral lytic factor protein VI (Wiethoff et al., 2005) by using CAR receptor drifts and integrin confinements (Burckhardt et al., 2011). Cytosolic particles engage in bidirectional microtubule-based transport to the nucleus (Bremner et al., 2009; Gazzola et al., 2009; Suomalainen et al., 1999), dock to the NPC protein Nup214, and attach the highly mobile nuclear histone H1 to acidic clusters of the major capsid protein hexon (Rux and Burnett, 2000; Trotman et al., 2001). Viral capsids are disassembled by an

unknown mechanism at the NPC, as revealed by a conformation-specific anti-hexon antibody or the dissociation of the internal core protein pV in case of a transgenic Ad2-GFP-pV (Puntener et al., 2011). Capsid fragments are left behind in the cytoplasm (Greber et al., 1997; Martin-Fernandez et al., 2004), and consequently, viral DNA enters the nucleus (Greber et al., 1997). Here, we found that the anterograde microtubule motor kinesin-1 disrupts NPC-docked capsids and surprisingly also the NPC, and opens access for the viral genome into the nucleus.

Results

Disassembled viral capsids in the cytoplasm are associated with nucleoporins

Immune-fluorescence analysis of cells infected with Texas-Red (TR)-labelled Ad2 particles using a polyclonal anti-capsid antibody (R70), which specifically detects disrupted but not intact Ad2 capsids after DNA-import into the nucleus (see Suppl. Fig. 1A, and Puntener et al., 2011; Trotman et al., 2001) reveals that the cell periphery is enriched in numerous R70-postive puncta at 180 min post infection (pi) (Fig. 1a). Thin section transmission electron microscopy (TEM) of infected cells at 180 min pi showed that cytosolic viral structures were significantly reduced in size compared to intact particles at the plasma membrane, or partly disrupted particles in endosomes 7 min pi (Fig. 1b, c). These structures often occurred in clusters and appeared as disrupted capsid clusters, indicated by correlative fluorescence microscopy and TEM (Suppl. Fig. S1A, b). Since capsid disassembly occurs at the NPC (Trotman et al., 2001), we tested if these viral puncta were positive for nucleoporins. By confocal microscopy, we found Nup358, Nup214 and Nup62 but not Nup153 on amorphous cytosolic capsid puncta, irrespective of whether the cells were treated with the protein synthesis inhibitor cycloheximide (Fig. 1d, e). The

capsids of a virus mutant Ad5-ΔpIX, which lacked the small capsid protein IX (pIX), was transported in the cytoplasm as wild type virus (Gazzola et al., 2009), had strongly reduced Nup358 and Nup62 signals, demonstrating that these Nups did not just randomly associate with the major capsid protein hexon (see Fig. 1e, and Suppl. Fig. S1B, a, b). Non-infected cells or cells infected for less than 60 min had no detectable Nups in the cell periphery (Suppl. Fig. S1B, c, data not shown). Similar to Nup358, Nup214 and Nup62, which occur in a complex (reviewed in Suntharalingam and Wente, 2003), the Nup358 binding protein RanGAP1 (Mahajan et al., 1997), and the nuclear export factor Crm1, which binds to Nup214 and Nup358 during nuclear export (Bernad et al., 2004; Hutten and Kehlenbach, 2006) localized to peripheral cytoplasmic Ad2 particles at 180 min pi (Suppl. Fig. S1B, d, Suppl. Fig. S1C, Suppl. Movie S1). There was no evidence for nucleoporin proteolysis by Western blot analyses of infected cell extracts (not shown), suggesting that nucleoporin colocalization with disrupted cytoplasmic Ad is not related to apoptotic proteolysis. None of the Nups tested, nor RanGAP1 or Crm1, however, were found on virus particles in cells treated with the Crm1 inhibitor leptomycin B (LMB), which blocks nuclear export and prevents viral localization to the nucleus (Suppl. Fig. S1B, e). Importantly, LMB not only blocked the appearance of R70 epitopes, but also the dissociation of the capsid protein GFP-pV from the virus particles, indicating that it blocked capsid disassembly (Puntener et al., 2011; Strunze et al., 2005).

To examine if the recruitment of nucleoporins and associated proteins to disrupted cytosolic Ad2 capsids occurred upon contact of the virus with the NPC at the nuclear envelope, we expressed the photo-convertible Kaede-Nup214 in HeLa cells for 48 h. Nup214 is one of the most stable Nups with an estimated NPC residence time of about 40 h (Daigle et al., 2001; Rabut et al., 2004). Kaede-Nup214 was incorporated into the nuclear envelope in a punctate pattern typical for NPCs (Suppl. Fig. S1D, a). Cells expressing Kaede-Nup214 were inoculated with Ad2-atto647 and the nucleus

photo-activated with 355 plus 405 nm light, according to previously described protocols (Ando et al., 2002). Non-converted Kaede-Nup214, converted Kaede-Nup214 and virus capsid fluorescence were imaged at 488, 561 and 633 nm excitation, respectively, at 90-160 min pi (Fig. 1f). From about 3000 analysed virus particles and 59 virus clusters (defined by a thresholding algorithm, see Suppl. Fig. S1D, b), we found 10 events of converted Kaede-Nup214 colocalization with clustered Ad2-atto647 (Fig. 1f, arrows; 17% positive clusters, Fig. 1g), and none with non-clustered Ad2-atto647, while non-converted Kaede-Nup214 colocalized with estimated less than 1% of non-clustered Ad2-att647 (Fig. 1f, double arrowheads). These data indicate a functional relationship between clustered (aggregated, disassembled) capsids in the cytosol and Kaede-Nup214 at the nuclear envelope.

Viral capsid disruption requires kinesin-1

Live cell analyses of Crm1-GFP expressing cells revealed Crm1-GFP positive Ad2 capsids in trajectories from the nuclear envelope to the periphery, reminiscent of microtubule dependent motions (see Suppl. Fig. S1C, Suppl. Movie S1). We examined whether disassembled capsids co-localized with kinesin-1 given the localization of viruses in the cell periphery, and the role of this anterograde microtubule motor in moving cellular and viral cargos, including vaccinia virus, African swine fever virus and Herpes viruses from the cell center to the periphery (reviewed in Greber and Way, 2006). We found that cytosolic capsid aggregates in the cell periphery were positive for kinesin light chain 1 (Klc1) as well as Klc2-GFP (Fig. 2a, b). GFP-Klc2 was observed on motile Ad2-TR virus particles moving in a linear and continuous fashion at µm/s velocities from the cell center to the periphery at 239 min pi, when most of the Ad2-TR particles were positive for Klc2-GFP (Suppl. Mov. S2). This is consistent with the observed speeds for kinesin-1 in single molecule studies (Watanabe et al., 2010).

The N-terminus of KLC1/2 is predicted to engage in coiled-coil interactions with the heavy chain of Kif5 (Mandelkow and Mandelkow, 2002), while the C-terminus contains six tetratricopeptide repeats (TPR) of about 34 amino acids and is involved in cargo binding interactions (Hirokawa et al., 2009). We used GFP fused to the TPR domain of Klc2 (which is very similar to that of Klc1), and could confirm that virus particles recruited kinesin-1 via the light chain (Fig. 2c). The colocalization of Ad2-TR with GFP-TPR not only increased from 0 to 30 min pi coincident with the arrival of particles in the cytosol and the very first particles at the nucleus, but more interestingly, after 60 min pi when most particles had reached the nucleus, and disassembly measurably commenced, GFP-TPR was increasingly found on R70-positive structures (Fig. 2D, Trotman et al., 2001). The over-expression of GFP-TPR, however, reduced the appearance of R70-positive capsids, and lowered infection by about 50%, suggesting that it worked as a dominant-negative for kinesin-1 function (Fig. 2e, f), as shown previously for vaccinia virus (Rietdorf et al., 2001). The reduction in the level of infection was not due to a lack of targeting to the nuclear envelope or entry of virus particles into the cytosol, as demonstrated by confocal fluorescence microscopy and TEM analysis (Suppl. Fig. S2A). In contrast to GFP-TPR, over-expression of GFP-tagged p50 dynamitin inhibited targeting of Ad2 to the nuclear envelope and infection (Suppl. Fig. S2A), consistent with the established role of dynein/dynactin complex in Ad2 transport to the nucleus (Bremner et al., 2009; Engelke et al., 2011; Suomalainen et al., 1999). These inhibition results together with the finding that there were only low levels of TPR-GFP on incoming Ad2-TR before disassembly (Fig. 2d), suggest that GFP-TPR inhibited infection after virus attachment to the nuclear pore complex due to blocking of kinesin-1 recruitment.

Given this result we tested the involvement of kinesin-1 in Ad2/5 infection by using small interfering RNAs (siRNAs) against kinesin light chain Klc1 and heavy chains Kif5B and Kif5C. RNA interference against Klc2 had no effect (not shown). Kif5B

and Kif5C are expressed in a variety of tissues and involved in morphogenetic processes and anterograde transport of mitochondria and vesicles in neuronal cells, although the function of Kif5C in epithelial cells is not known (reviewed in Astanina and Jacob, 2010). siRNA against Klc1 and Kif5C but not Kif5B reduced Ad2 infection and capsid uncoating (Fig. 2g-i). All the siRNAs reduced the corresponding mRNAs as determined by quantitative PCR, and did not affect the delivery of Ad2 particles to the cytosol (Suppl. Fig. S2B, not shown). These observations suggest that Klc1/2 and Kif5C are associated with Ad2 particles, particularly disassembled capsids in the cytoplasm, and are required for infectious capsid disassembly at the nuclear envelope.

Kinesin light chain binds protein IX of intact and disrupted particles

To address how kinesin-1 is recruited to the virus particles, we incubated triple CsCl-purified intact or heat-disrupted Ad2 particles with GST-TPR or GST alone (Fig. 3a, top two panels). Ad2 particles were disassembled by heat disruption, which opens up the capsids and releases internal pV (Puntener et al., 2011). Western blot analysis against hexon revealed that GST-TPR immobilized on glutathione-sepharose beads or GST-Klc2 (not shown), but not GST pulled down Ad2 particles or hexon from heat disrupted particles (Fig. 3a, third panel from top). Heat disruption gave rise to capsomers, including the group of nine hexons stabilized by pIX (Fig. 3B inset, and, Liu et al., 2010). Similarly, biotinylated Ad2 on streptavidin-coated beads bound GST-TPR but not GST (Fig. 3c).

To determine which viral protein is responsible for recruiting kinesin-1 we analysed the profile of [^{35}S]-methionine viral proteins from heat denatured Ad2 that were capable of binding GST-TPR. GST-TPR pulled down major fractions of hexon (II), the capsid stabilizing proteins IIIa and IX and small amounts of fiber (IV) (Fig. 3a, lowest panel, * symbols). Control pull-downs with intact Ad2 yielded the complete

spectrum of virion proteins (Fig. 3a, lowest panel). We focussed our attention on pIX, since pIIIa and fiber are shed from the incoming virions at the plasma membrane and endosomes (Greber et al., 1993). pIX is conserved in mammal-tropic mastadenoviruses (Davison et al., 2003). Moreover, the localization of pIX on the virus is consistent with a potential interaction with Klc1/2, as its N-terminus and the central domain tightly adhere to the outside of the virion, and the C-terminus projects away from the surface of the virus (Liu et al., 2010).

Immune-precipitation of myc-tagged pIX from lysates of transfected cells confirmed that pIX interacts with HA-tagged Klc1 (Fig. 3d). An interaction between the two proteins was further supported by the observation that Ad5-ΔpIX (Vellinga et al., 2005) or purified hexon bound about ~20-times less to GST-TPR than wild type Ad5 as determined by densitometric scanning (Fig. 3e). The sequence of pIX of Ad2 and Ad5 are 100% conserved except for amino acid residue three. This contrasts the major antigenic determinants, hexon and fiber, which have 87% and 69% identities between Ad2 and Ad5 serotypes, respectively. The almost 100% sequence conservation of pIX suggests that the protein plays an important but undefined role during virus infection. Given this, we examined if pIX has a role in infection, as measured by accumulation of newly synthesized viral antigens in the nucleus. Infection of HeLa cells with Ad5-ΔpIX was significantly reduced compared to wild-type Ad5, although Ad5-ΔpIX particles localized to the nucleus with similar or even higher efficiency compared to Ad5 (Fig. 3f, g). Our observations are consistent with an earlier report showing that the reduced infectivity of Ad5-ΔpIX was independent of a putative transcriptional activity of pIX, and that pIX-deficient Ad2 were impaired in viral propagation (Sargent et al., 2004). Collectively, the data show that Klc1/2 binds to pIX, and supports the infectious uncoating of incoming virus particles.

Kif5C attachment to Nup358 supports infectious virus disassembly

Previous observations showed that Kif5C heavy chain interacts with the kinesin binding domain JX2 of Nup358 (Cho et al., 2007), which is anchored to Nup214 of the NPC (reviewed in D'Angelo and Hetzer, 2008), and extends approximately 150 nm from the nuclear membrane into the cytoplasm. We tested if attachment of Ad2 to the NPC was required for uncoating and infection. Knock-down of the adenovirus docking site Nup214 by RNA-interference inhibited targeting of Ad2-atto565 to the nuclear envelope similarly as treatment with the microtubule-depolymerizing agent nocodazole, while knock-down of Nup358 had no effect, although the knock-down of Nup358 was stronger than Nup214 (Suppl. Fig. S3). In contrast, Nup214 or Nup358 knock-down inhibited the uncoating of Ad2-GFP-pV, as indicated by increased GFP-pV in the Ad2 capsids at 150 min pi compared to no or scrambled siRNA treated cells (Fig. 4a, b, and not shown), and blocked the peripheral R70 signals (not shown). These data indicate that adenovirus infection requires Nup214 and Nup358 for uncoating, but only Nup214 is involved in viral attachment to the NPC.

We next tested if Nup358 and kinesin-1 were functionally linked with each other. Using cryo-immune-electron microscopy employing the Kif5C/5A specific antibody H1 (which reacts with the major form of heavy chain of non-neuronal KHC near the N-terminus), we found that Kif5C/5A was associated to Ad2-free NPCs, or NPCs containing docked Ad2 (Fig. 5a). Quantification of immune-gold from samples that were not treated with the H1 antibody indicated that the labelling for kinesin-1 was specific (Fig. 5b). Since Kif5A does not bind to Nup358 (Cho et al., 2007), these data suggested that Kif5C localizes to the NPC independently of Ad2. The knockdown of Nup358 reduced Ad5-mediated GFP expression from 51.1% to 19.7% (Fig. 5c, d). The ratios of GFP expression in transfected over non-transfected cells were 2.4 for empty plasmid control, and 0.65 for the plasmid encoding Nup358 interfering RNA (quadrant 2 divided by quadrant 4), indicating a nearly 4-fold inhibition of infection by Nup358 interference. Expression of Nup358 interfering RNA

inhibited the appearance of peripheral R70-positive capsids, but did not affect the localization of incoming Ad2-TR at the nuclear envelope (Fig. 5c, e). Importantly, Nup358 was not required for expression of GFP from herpes simplex virus, but specifically for adenovirus, indicating that Nup358 depletion did not affect viral gene expression non-specifically (Suppl. Fig. S4). This is consistent with the observation that HSV1 uses Nup214 rather than Nup358 for attachment to the NPC (Copeland et al., 2009; Pasdeloup et al., 2009). Further to the requirement of full length Nup358, Ad2-mRFP transduction was inhibited by the expression of the JX2 domain of Nup358 fused to GFP (Fig. 5f). JX2 binds to and activates kinesin-1 (Cho et al., 2009), suggesting that active kinesin-1 at Nup358 is required to enhance infection. This result was strengthened by the observation that Ad2-mRFP transduction was also inhibited by over-expressing a monomeric N-terminal motor domain construct of Kif5C (amino acids 1-332) that lacks the Nup358 binding domain (amino acids 827–923). Together, these data indicate that an interaction of Kif5C with the JX2 domain of Nup358 supports adenovirus infection, but is not required for localization of the virus to the nuclear envelope.

The displacement of Nups from the NPC increases infection and nuclear envelope permeability

So far, the data indicated that the kinesin-1 motor protein binds to the viral capsid and the NPC, releases nucleoporins from the nuclear envelope during capsid disruption, and thereby disperses capsid-nucleoporin complexes to the cell periphery, and promotes infection. To test if the loss of nucleoporins from NPCs disrupted the integrity of the nuclear envelope, we microinjected inert fluorescent dextran molecules into the cytoplasm of HeLa cells, infected the cells for up to 180 min, and measured the steady state distribution of dextran fluorescence in the nucleus and the cytoplasm by live cell confocal fluorescence microscopy. While the gel-filtration purified 2000 kDa dextran-tetramethylrhodamine (TMR, fractions f27-32) remained excluded from the nucleus, 500 kDa dextran-fluorescein-

isothiocyanate (FITC, f44-49, comprising dextrans that are slightly smaller than the peak of the 500 kDa dextran-FITC, see supplemental information) and the broad range 40 kDa dextran-FITC (eluting in fractions 35-64) were found in the nucleus of infected but not uninfected cells (Fig. 6a-e). The 40 kDa dextran-FITC is near the diffusion barrier of the NPC, whereas larger dextrans enter the nucleus only, when the NPCs are disrupted (Lenart and Ellenberg, 2006; Mohr et al., 2009). Our results therefore suggest that the NPCs of adenovirus-infected cells are partly disrupted. Interestingly, this disruption was transient, since cells infected for 240 min prior to injection of the broad range 40 kDa dextran-FITC excluded the dextran from the nucleus even stronger than non-infected cells (Fig. 6e).

To test if virus docking to the NPC was required to trigger nuclear leakage, we treated cells with the nuclear export inhibitor LMB, which blocks virus docking to the NPC (Strunze et al., 2005). LMB inhibited the influx of the broad range 40 kDa dextran, although it did not block it completely (Fig. 6e). These results were confirmed in cells treated with siRNAs against the adenovirus docking receptor Nup214 or the kinesin receptor Nup358, both of which strongly inhibited virus-induced nuclear leakage of 40 kDa dextran-FITC (Fig. 6f). Neither the knock-down of Nup214 nor Nup358 induced significant nuclear leakage by itself, implying that multiple Nups may be displaced by adenovirus to allow dextran influx. We also tested if the kinesin-light chain binding protein pIX was involved in nuclear envelope disruption. Infection with Ad5ΔpIX, which did not recruit Nup358 and was not clustered in the cell periphery (Fig. 1e, and Suppl. Fig. S1B), did not significantly increase the nucleo-cytoplasmic ratio of 40 kDa dextran-FITC. The results indicate that pIX is not only important for capsid disassembly, but also for increasing the permeability of the nuclear envelope during virus entry (Fig. 6g).

Discussion

How viruses transport and activate their genome in the nucleus has been a long-standing question in infectious disease biology. Genome activation invariably requires uncoating from a protecting protein shell, which, however, triggers potent innate immune responses against the exposed viral nucleic acids (reviewed in Wilkins and Gale, 2010).

Here, we found a novel microtubule motor-based mechanism for uncoating of adenoviral DNA, for disrupting the NPCs and facilitating nuclear import of viral DNA (Fig. 7). Adenoviruses undergo a stepwise uncoating program, which culminates with DNA release into the nucleus (Greber et al., 1993). Since we see very little colocalization of kinesin-1 with incoming virus particles and interference with kinesin-1 or the kinesin-1 binding partner of the virus, pIX have no negative effects on targeting the virus to the nuclear envelope, we suggest that subviral capsids recruit kinesin-1 at the NPC. At the NPC docking site Nup214, the subviral capsid is largely composed of the major capsid protein hexon and viral DNA. The hexon facettes are stabilized by multiple copies of pIX, and the viral DNA condensed by proteins pVII, pV and pX (Puntener et al., 2011). The particle becomes subject to a pulling force from the Kif5C heavy chain. Kif5C is activated by its binding partner Nup358 (Cho et al., 2009), and tethered to the particle by Klc1, which binds pIX. The particle thereby acts as a cooperative scaffolder, and engages multiple kinesin-1 motors, which could move on NPC-proximal microtubules (Joseph and Dasso, 2008). This explains an earlier observation, namely, why nocodazole-induced loss of microtubules inhibited infection both during cytoplasmic transport and thereafter (Mabit et al., 2002). Particle disruption presumably results in the release of group of nine hexon trimers (GONs), still stabilized by pIX (Liu et al.; Reddy et al., 2010).

Some of the GONs may remain bound to Nup214, and continue to be subject to pulling forces by kinesin-1. Hexon binding to Nup214 may weaken the anchoring of Nup214 in the NPC, and thereby help to disrupt parts of the cytoplasmic structure of the NPC.

The work here sheds new light on how viral nucleic acids take advantage of the NPC to get access to the nucleus. The NPC is a selective gateway for proteins, nucleic acids and solutes in and out of the nucleus. The FG-repeat barrier works by hydrophobic exclusion, and is particularly effective for very large molecules. Remarkably, the action of kinesin-1 at the NPC-docked virus disrupts the integrity of the NPC. This observation is similar, but mechanistically distinct from a report showing an increase of nuclear envelope permeability from aged nuclei as a consequence of oxidation and proteolytic removal of Nup93 (D'Angelo et al., 2009). In both instances, viral infection and aged nuclei, signal-mediated nuclear import is not impaired (D'Angelo et al., 2009; Trotman et al., 2001). This is consistent with genetic deletion studies of FG and GLFG repeats of yeast Nups, which showed that NPC functionality is maintained in the absence of up to half of the FG-repeat mass (Strawn et al., 2004). It is also reminiscent of mitotic *Aspergillus nidulans* cells, where most of the NPC-peripheral Nups are dispersed to the cytoplasm, which leaves behind a minimal functional NPC (Osmani et al., 2006). Our results are distinct from the mitotic breakdown of NPCs, as driven by CDK1 and NIMA-related kinase-mediated phosphorylation of Nup98 (Laurell et al., 2011).

We have directly measured the disruption of the NPC integrity by the displacement of both central and peripheral Nups, which comprise cohesive and non-cohesive Nups to stabilize the NPC (Alber et al., 2007; Galy et al., 2003). Interestingly, the displacement of FG-containing Nups increased the nuclear envelope permeability for hydrophilic dextran molecules. This is in agreement with studies in yeast, where

genetic deletions of individual FG-domains relaxed the NPC permeability barrier (Patel et al., 2007). Recent diffusion measurements of solutes have further suggested that the transit of relatively hydropobic receptor-cargo complexes and solutes occurs at least in part through the same channels built up by FG-repeat proteins (Mohr et al., 2009). The displacement of FG-containing Nups by adenovirus could hence enhance the import of the viral DNA-genome through the diffusion channels. This is supported by the transient nature of the relaxed diffusion barrier, which argues that the viral DNA-protein complex competes with solutes for passage through the NPC.

Adenovirus DNA import also takes advantage of carrier-mediated transport mechanisms. The viral genome is a linear DNA of about 36 kbp, condensed into 140-180 nucleosome-like structures by the dimeric protein VII, the minor protein X, and the accessory protein pV (Chatterjee et al., 1985; Chen et al., 2007; Corden et al., 1976; Puntener et al., 2011; van Oostrum and Burnett, 1985). Since pVII but not pV remains associated with the DNA until import is completed (Puntener et al., 2011; Xue et al., 2005), several hundred import receptors are thought to cover the highly charged DNA-protein complex. Opening up of the diffusion channels prior to or during nuclear import could make DNA import less dependent on nuclear import factors. Importins beta1, beta2 and 7 are known to be limiting for adenovirus infection, as suggested by antibody microinjection studies or cell free import assays (Hindley et al., 2007; Trotman et al., 2001), and mediate the import of the viral core associated protein VII (Wodrich et al., 2006).

Collectively, by showing that kinesin-1 can disrupt both viral capsids and the NPC we extend the known function(s) of kinesin motors, and uncover a novel way to get cargo into the nucleus. Our findings specifically define new roles for kinesin-1 and Nup358 in viral infections at the NPC. This could be of interest also for other viruses,

such as HIV, where Gag associates with Kif4, a member of the N-terminal kinesin superfamily (Tang et al., 1999), and Nup358 and Nup153 have potential roles for provirus formation in the nucleus (Brass et al., 2008).

Experimental procedures

Detailed experimental procedures are described in the Supplemental Materials.

Acknowledgements

We thank Dr.'s Brian Burke, Maarten Fornerod, Silvio Hemmi, Rob Hoeben, Ulrike Kutay, Frauke Melchior, Kevin Pfister, Cornel Fraefel and Manuel Rosa-Calatrava for reagents or virus stocks, Maarit Suomalainen and Corinne Wilhelm for help with dextran purification and Western blotting. This work was supported by the Swiss National Science Foundation (UFG), the Kanton Zürich (UFG) and Cancer Research UK (MW). The authors declare no competing financial interests.

Figure legends

Figure 1: Nucleoporins are picked up from the nuclear envelope by the incoming virus and transported on disassembled capsids to the periphery

a) Clusters of disassembled Ad2-TR stained by the conformation sensitive anti-hexon antibody R70 in the cytoplasm and cell periphery 180 min pi.

b) Disassembled cytosolic capsids (arrow-heads) are smaller than extracellular viruses (arrows) analysed by EM at 0 min (cold-bound viruses) or 180 min pi. See also Suppl. Fig. S1A.

c) Mean values of capsid diameters including SEM and number of capsids (n) analysed from 2 independent experiments.

d) Displacement of Nup358, Nup214 and Nup62 to the cytoplasm in the presence of 0.1 mg/ml cycloheximide 180 min pi. Fixed cells were analysed by single section CLSM with cell borders outlined from DIC images. See also Suppl. Fig. S1B and S1C, and Suppl. Movie S1.

e) Quantification of immune-stained Nup358, Nup62 and Nup153 colocalizing with cytoplasmic Ad5-atto565 and Ad5ΔpIX-atto565, respectively, normalized for atto565 signal. n = number of analysed cells from 2 independent experiments.

f) Localization of photo-converted Kaede-Nup214 from the nuclear envelope area to cytoplasmic clusters of virus capsids 160 min pi. A merged triple color image from confocal sections shows non-converted Kaede-Nup214 (green), Ad2-atto647 (blue) and photo-converted Kaede-Nup214 (red) with corresponding single channels of a cytoplasmic area of interest (boxed), and the outline of the corresponding cell determined from the DIC image (white line, not shown). The arrows indicate Ad2-atto647 clusters, which are positive for photo-converted and negative for non-converted Kaede-Nup214. Arrowheads (in the main image) point to puncta of converted and non-converted Kaede-Nup214 with sub-threshold levels of Ad2-

atto647. Double arrowheads point out a minority of Ad2-atto647 particles double positive for converted and nonconverted Kaede-Nup214. Stars (*) mark photoactivated nuclei from three different cells. See also Suppl. Fig. S1D.

g) Quantification of Ad2 particles positive for photo-converted Kaede-Nup214 (cK-Nup214), including Ad2 clusters and total number of Ad2 particles in 6 different photo-converted cells expressing Kaede-Nup214.

Figure 2: Kinesin-1 supports adenovirus disassembly and infection

a) Immune-fluorescence analysis of incoming Ad2-TR reveals co-localization with endogenous Klc1 in the cell periphery 150 min pi.

b) Colocalization of Ad2-TR with transiently expressed Klc2-GFP in the cell periphery near microtubules 180 min pi. See also Suppl. Movie S2.

c) Transiently expressed GFP-TPR colocalizes with disassembled Ad2-TR particles (arrowheads) visualized by R70 stainings, unlike intact Ad2 (arrows) in the cell periphery 180 min pi.

d) GFP-TPR colocalization with R70-positive particles increases with infection time (yellow bars), but GFP-TPR colocalization with R70-negative Ad2-TR remains constant 30 min pi (red bars). Representative mean values from several independent experiments including SEMs are shown.

e) Inhibition of virus disassembly in GFP-TPR expressing cells measured by R70 stainings.

f) Inhibition of Ad2–mRFP infection by over-expression of GFP-TPR, analysed by single cell confocal microscopy 12h pi. See also Suppl. Fig. S2A.

g, h) siRNA-mediated knock-down of Klc1 or Kif5C reduces Ad2-mRFP expression compared to non-silencing (n.sil.) or Kif5B siRNAs, measured by flow cytometry 12h pi. For statistical details, see also Suppl. Fig. S2B.

i) Knock-down of Klc1 or Kif5C reduces Ad2 disassembly measured by R70 staining.

Figure 3: Ad2 binds the TPR domain of Klc1/2 through the capsid protein pIX

a) Intact or heat disrupted [^{35}S]-methionine-labeled Ad2 particles were incubated with recombinant GST-TPR or GST on glutathione-Sepharose, washed and analysed by Western blotting against GST (top two rows), agains hexon (third row) or autoradiography (fourth row). Note that GST-TPR bound similar amounts of hexon and pIX from both intact and heat disrupted virions but less penton base (III), fiber (IV) and inner capsid proteins (V, VI, VII, VIII) from heat-ruptured than intact virions.

b) Transmission electron micrographs of purified viruses stained with uranyl acetate reveal groups of nine hexons (GONs, inset) of heat disrupted Ad2 but not purified hexon, which is free of pIX (not shown).

c) Binding of biotinylated Ad2 to GST-TPR-glutathione-Sepharose measured by Western blotting against GST and hexon.

d) Co-immune-precipitation of HA-tagged Klc1 with myc-tagged pIX. HEK293T cells were transfected with the indicated constructs, cell lysates immune-precipitated with anti-pIX antibodies, and immuncomplexes blotted with anti-myc (upper panel) and anti-KLC antibodies (lower panel). Input panels are shown below the blots.

e) Ad5 and much less Ad5-ΔpIX capsids or HPLC-purified hexon protein bind to GST-TPR as indicated by GST pulldown experiments and Western blotting against hexon and pIX. Relative molecular weights are indicated in kDa.

f) Analyses of subcellular localization of fluorescent Ad5 and Ad5-ΔpIX indicate that pIX is not required for cytoplasmic transport of the virus to the nuclear envelope. The y-axis plots the fluorescence of virus particles normalized per unit area. n indicates number of cells analysed, and error bars SEM values.

g) pIX is required for efficient Ad5-mediated gene expression. Human embryonic retinoblast 911 cells were infected with different amounts of Ad5-wt and Ad5-ΔpIX, and analysed for penton base and fiber expression by confocal microscopy 15h pi (mean values of triplicates, with SEMs; moi = multiplicity of infection upon cold synchronization).

Figure 4: Nup358 or Nup214 are required for the release of GFP-pV from adenovirus

a) Human embryonic retinoblast 911 cells were treated with siRNAs against Nup358 or Nup214 and infected with atto647 labeled Ad2-GFP-pV for 30 min or 150 min, fixed and analysed for capsid (atto647) and GFP fluorescence. Ad2-GFP-pV virions contain about 38 GFP-pV molecules of which about two thirds are released within the first 30 min during virus entry, and one third at the NPC (Puntener et al., 2011).

b) Table with the mean of GFP-pV fluorescence per Ad2-atto647, including number of viruses, cells, experiments (n), standard errors, and p-values compared to no siRNA treated cells. See also Suppl. Fig. S3.

Figure 5: NPC-localized Kif5C supports viral disassembly

a) Kif5C localizes to NPC-docked Ad2. HeLa cells infected with Ad2 for 60 min, were processed for cryo-immune-electron microscopy using the Kif5A/C-specific mouse monoclonal antibody Mab H1. Immune-gold-labeled Kif5C (arrows) was found at Ad2-docked NPCs (arrow heads) less than 200 nm away from the virions and the nuclear membrane (panel 1). Little gold particles were detected in samples incubated without Mab H1 (panel 2).

b) Left side depicts the quantification of Kif5A/C gold particles at the nuclear envelope (NE) in noninfected cells (no Ad), or at the nuclear envelope of infected cells in close proximity to Ad2 particles (<200 nm) (Ad2). The numbers of Ad2

particles at the nuclear envelope (normalized per cells, cell number = 18) with or without Mab H1 staining is shown as a pair of columns on the right side.

c) Knock-down of Nup358 does not reduce transport of Ad2-TR to the nucleus. Cells transfected with pS-Nup358 for 84h were infected with Ad2-TR for 80 min, fixed and processed for immune-fluorescence staining using anti-Nup358 antibodies. Nup358 knock-down cells are pointed out by arrows. Note the reduced amounts of Ad2-TR in the periphery of Nup358 knock-down cells. Total intensity projections of confocal stacks including DAPI stainings are shown. See also Suppl. Fig. S4.

d) Knock down of Nup358 reduces the transduction of Ad5-GFP. HeLa cells were co-transfected with pS-Nup358 and mRFP encoding plasmids, infected with Ad5-GFP, fixed at 6h pi, and analysed by flow cytometry. The upper right quadrant shows transfected cells (mRFP-positive) that are infected (GFP-positive).

e) pS-Nup358 mediated knock-down of Nup358 inhibits Ad2 capsid disassembly compared to empty vector pS (pSuper), measured with the disassembly-specific anti-hexon antibody R70. Graphs represent mean values of analysed samples (n) including the SEM, and p-values from t-tests.

f) Expression of the kinesin heavy chain binding domain JX2-GFP derived from Nup358, or dominant-negative (dn) Kif5C-GFP reduces Ad2-mediated mRFP expression 12h pi. Graphs represent mean values of analysed samples (n) including the SEM, and p-values from t-tests.

Figure 6: Adenovirus mediated disruption of the NPC leads to dextran influx into the nucleus

a, b) HeLa cells microinjected with a mixture of gel filtration-fractionated large sized dextran-TMR (f27-32) and medium sized dextran-FITC (f44-49) were inoculated with Ad2 for 180 min, imaged by live cell spinning disc confocal fluorescence microscopy and analysed for nuclear and cytoplasmic dextran.

c) Cells microinjected with broad range 40 kDa dextran-FITC were infected and imaged as described for a).

d) Analytical gel filtration profiles of injected 500 kDa dextran-FITC and 2000 kDa dextran-TMR, fractionated by Superose 6-HR 10/30 column, as well as broad range (non-fractionated) 40 kDa dextran-FITC.

e) HeLa cells injected with broad range 40 kDa dextran-FITC were either treated or not with 20 nM leptomycin B (LMB), infected and imaged as outlined in a). Mean values of cytoplasmic to nuclear ratios are shown for infected cells (Ad2, black bars) or non-infected cells (open bars). Cells were also first infected with Ad2 for 240 min, and then injected with 40 kDa dextran-FITC (grey bar).

f) Mean values of cytoplasmic to nuclear ratios of cells treated with siRNA against Nup214, Nup358, or scrambled siRNA (SCR), microinjected with broad range 40 kDa dextran-FITC and infected or not infected.

g) Ratios of cytoplasmic to nuclear dextran in cells microinjected with the broad range 40 kDa dextran-FITC and infected with Ad5 or Ad5ΔpIX.

All graphs represent mean values of analysed samples (n) including the SEM, and p-values from t-tests.

Figure 7: Model for kinesin-1 mediated virus disassembly at the NPC

Incoming adenovirus (red) traffics towards the nucleus using the microtubule minus end-directed motor complex dynein/dynactin, and attaches to the NPC by hexon interactions with Nup214. Viral capsids bind to the kinesin-1 light chain Klc1/2 by the hexon-associated pIX. Nup358 attached to the Nup214/Nup88 complex (reviewed in D'Angelo and Hetzer, 2008) associates with kinesin-1 heavy chain Kif5C via the JX2 domain, and possibly with microtubules through a distal microtubule-binding domain. Kinesin-1 motors disrupt the viral capsid, and dislocate Nup358/Nup214 and Nup62

from the central NPC channel to the periphery. The disruption of the NPC facilitates entry of the viral DNA into the nucleus.

References

Alber, F., Dokudovskaya, S., Veenhoff, L.M., Zhang, W., Kipper, J., Devos, D., Suprapto, A., Karni-Schmidt, O., Williams, R., Chait, B.T., *et al.* (2007). The molecular architecture of the nuclear pore complex. Nature *450*, 695-701.

Ando, R., Hama, H., Yamamoto-Hino, M., Mizuno, H., and Miyawaki, A. (2002). An optical marker based on the UV-induced green-to-red photoconversion of a fluorescent protein. Proc Natl Acad Sci U S A *99*, 12651-12656.

Astanina, K., and Jacob, R. (2010). KIF5C, a kinesin motor involved in apical trafficking of MDCK cells. Cell Mol Life Sci *67*, 1331-1342.

Bernad, R., van der Velde, H., Fornerod, M., and Pickersgill, H. (2004). Nup358/RanBP2 attaches to the nuclear pore complex via association with Nup88 and Nup214/CAN and plays a supporting role in CRM1-mediated nuclear protein export. Mol Cell Biol *24*, 2373-2384.

Brass, A.L., Dykxhoorn, D.M., Benita, Y., Yan, N., Engelman, A., Xavier, R.J., Lieberman, J., and Elledge, S.J. (2008). Identification of host proteins required for HIV infection through a functional genomic screen. Science *319*, 921-926.

Bremner, K.H., Scherer, J., Yi, J., Vershinin, M., Gross, S.P., and Vallee, R.B. (2009). Adenovirus transport via direct interaction of cytoplasmic dynein with the viral capsid hexon subunit. Cell Host Microbe *6*, 523-535.

Burckhardt, C., Suomalainen, M., Schoenenberger, P., Boucke, K., Hemmi, S., and Greber, U. (2011). Drifting motions of CAR and immobile integrins initiate adenovirus uncoating and expose the membrane active virion protein VI. Cell Host & Microbe *in press*.

Cai, Y., Singh, B.B., Aslanukov, A., Zhao, H., and Ferreira, P.A. (2001). The docking of kinesins, KIF5B and KIF5C, to Ran-binding protein 2 (RanBP2) is mediated via a novel RanBP2 domain. J Biol Chem *276*, 41594-41602.

Chatterjee, P.K., Vayda, M.E., and Flint, S.J. (1985). Interactions among the three adenovirus core proteins. J Virol *55*, 379-386.

Chen, J., Morral, N., and Engel, D.A. (2007). Transcription releases protein VII from adenovirus chromatin. Virology *369*, 411-422.

Cho, K.I., Cai, Y., Yi, H., Yeh, A., Aslanukov, A., and Ferreira, P.A. (2007). Association of the kinesin-binding domain of RanBP2 to KIF5B and KIF5C determines mitochondria localization and function. Traffic *8*, 1722-1735.

Cho, K.I., Yi, H., Desai, R., Hand, A.R., Haas, A.L., and Ferreira, P.A. (2009). RANBP2 is an allosteric activator of the conventional kinesin-1 motor protein, KIF5B, in a minimal cell-free system. EMBO Rep *10*, 480-486.

Copeland, A.M., Newcomb, W.W., and Brown, J.C. (2009). Herpes simplex virus replication: roles of viral proteins and nucleoporins in capsid-nucleus attachment. J Virol *83*, 1660-1668.

Corden, J., Engelking, H.M., and Pearson, G.D. (1976). Chromatin-like organization of the adenovirus chromosome. Proc Natl Acad Sci U S A *73*, 401-404.

D'Angelo, M.A., and Hetzer, M.W. (2008). Structure, dynamics and function of nuclear pore complexes. Trends Cell Biol *18*, 456-466.

D'Angelo, M.A., Raices, M., Panowski, S.H., and Hetzer, M.W. (2009). Age-dependent deterioration of nuclear pore complexes causes a loss of nuclear integrity in postmitotic cells. Cell *136*, 284-295.

Daigle, N., Beaudouin, J., Hartnell, L., Imreh, G., Hallberg, E., Lippincott-Schwartz, J., and Ellenberg, J. (2001). Nuclear pore complexes form immobile networks and have a very low turnover in live mammalian cells. J Cell Biol *154*, 71-84.

Davison, A.J., Benko, M., and Harrach, B. (2003). Genetic content and evolution of adenoviruses. J Gen Virol *84*, 2895-2908.

Engelke, M.F., Burckhardt, C.J., Morf, M.K., and Greber, U.F. (2011). The Dynactin Complex Enhances the Speed of Microtubule-Dependent Motions of Adenovirus Both Towards and Away from the Nucleus. Viruses *3*, 233-253.

Frey, S., and Gorlich, D. (2007). A saturated FG-repeat hydrogel can reproduce the permeability properties of nuclear pore complexes. Cell *130*, 512-523.

Galy, V., Mattaj, I.W., and Askjaer, P. (2003). Caenorhabditis elegans nucleoporins Nup93 and Nup205 determine the limit of nuclear pore complex size exclusion in vivo. Mol Biol Cell *14*, 5104-5115.

Gazzola, M., Burckhardt, C.J., Bayati, B., Engelke, M., Greber, U.F., and Koumoutsakos, P. (2009). A stochastic model for microtubule motors describes the in vivo cytoplasmic transport of human adenovirus. PLoS Comp Biol *5*, e1000623.

Greber, U.F., Suomalainen, M., Stidwill, R.P., Boucke, K., Ebersold, M., and Helenius, A. (1997). The role of the nuclear pore complex in adenovirus DNA entry. EMBO J *16*, 5998-6007.

Greber, U.F., and Way, M. (2006). A super highway to virus infection. Cell *124(4)*, 741-754.

Greber, U.F., Willetts, M., Webster, P., and Helenius, A. (1993). Stepwise dismantling of adenovirus 2 during entry into cells. Cell *75*, 477-486.

Hayashi, S., and Hogg, J.C. (2007). Adenovirus infections and lung disease. Curr Opin Pharmacol *7*, 237-243.

Hindley, C.E., Lawrence, F.J., and Matthews, D.A. (2007). A role for transportin in the nuclear import of adenovirus core proteins and DNA. Traffic *8*, 1313-1322.

Hirokawa, N., Noda, Y., Tanaka, Y., and Niwa, S. (2009). Kinesin superfamily motor proteins and intracellular transport. Nat Rev Mol Cell Biol *10*, 682-696.

Hutten, S., and Kehlenbach, R.H. (2006). Nup214 is required for CRM1-dependent nuclear protein export in vivo. Mol Cell Biol *26*, 6772-6785.

Joseph, J., and Dasso, M. (2008). The nucleoporin Nup358 associates with and regulates interphase microtubules. FEBS Lett *582*, 190-196.

Kojaoghlanian, T., Flomenberg, P., and Horwitz, M.S. (2003). The impact of adenovirus infection on the immunocompromised host. Rev Med Virol *13*, 155-171.

Laurell, E., Beck, K., Krupina, K., Theerthagiri, G., Bodenmiller, B., Horvath, P., Aebersold, R., Antonin, W., and Kutay, U. (2011). Phosphorylation of Nup98 by multiple kinases is crucial for NPC disassembly during mitotic entry. Cell *144*, 539-550.

Lee, K., Ambrose, Z., Martin, T.D., Oztop, I., Mulky, A., Julias, J.G., Vandegraaff, N., Baumann, J.G., Wang, R., Yuen, W.*, et al.* (2010). Flexible use of nuclear import pathways by HIV-1. Cell Host Microbe *7*, 221-233.

Lenart, P., and Ellenberg, J. (2006). Monitoring the permeability of the nuclear envelope during the cell cycle. Methods *38*, 17-24.

Lim, R.Y., Fahrenkrog, B., Koser, J., Schwarz-Herion, K., Deng, J., and Aebi, U. (2007). Nanomechanical basis of selective gating by the nuclear pore complex. Science *318*, 640-643.

Liu, H., Jin, L., Koh, S.B., Atanasov, I., Schein, S., Wu, L., and Zhou, Z.H. (2010). Atomic structure of human adenovirus by cryo-EM reveals interactions among protein networks. Science *329*, 1038-1043.

Lowe, A.R., Siegel, J.J., Kalab, P., Siu, M., Weis, K., and Liphardt, J.T. (2010). Selectivity mechanism of the nuclear pore complex characterized by single cargo tracking. Nature.

Lutschg, V., Boucke, K., Hemmi, S., and Greber, U. (2011). Chemotactic anti-viral cytokines promote infectious apical entry of human adenovirus into polarized epithelial cells. Nature Communications *in press*.

Mabit, H., Nakano, M.Y., Prank, U., Saam, B., Döhner, K., Sodeik, B., and Greber, U.F. (2002). Intact microtubules support adenovirus and herpes simplex virus infections. J Virol *76*, 9962-9971.

Mahajan, R., Delphin, C., Guan, T., Gerace, L., and Melchior, F. (1997). A small ubiquitin-related polypeptide involved in targeting RanGAP1 to nuclear pore complex protein RanBP2. Cell *88*, 97-107.

Mandelkow, E., and Mandelkow, E.M. (2002). Kinesin motors and disease. Trends Cell Biol *12*, 585-591.

Martin-Fernandez, M., Longshaw, S.V., Kirby, I., Santis, G., Tobin, M.J., Clarke, D.T., and Jones, G.R. (2004). Adenovirus Type-5 Entry and Disassembly Followed in Living Cells by FRET, Fluorescence Anisotropy, and FLIM. Biophys J *87*, 1316-1327.

Mohr, D., Frey, S., Fischer, T., Guttler, T., and Gorlich, D. (2009). Characterisation of the passive permeability barrier of nuclear pore complexes. Embo J *28*, 2541-2553.

Newcomb, W.W., Juhas, R.M., Thomsen, D.R., Homa, F.L., Burch, A.D., Weller, S.K., and Brown, J.C. (2001). The UL6 gene product forms the portal for entry of DNA into the herpes simplex virus capsid. J Virol *75*, 10923-10932.

Osmani, A.H., Davies, J., Liu, H.L., Nile, A., and Osmani, S.A. (2006). Systematic deletion and mitotic localization of the nuclear pore complex proteins of Aspergillus nidulans. Mol Biol Cell *17*, 4946-4961.

Pante, N., and Kann, M. (2002). Nuclear pore complex is able to transport macromolecules with diameters of about 39 nm. Molecular Biology of the Cell *13*, 425-434.

Pasdeloup, D., Blondel, D., Isidro, A.L., and Rixon, F.J. (2009). Herpesvirus capsid association with the nuclear pore complex and viral DNA release involve the nucleoporin CAN/Nup214 and the capsid protein pUL25. J Virol *83*, 6610-6623.

Patel, S.S., Belmont, B.J., Sante, J.M., and Rexach, M.F. (2007). Natively unfolded nucleoporins gate protein diffusion across the nuclear pore complex. Cell *129*, 83-96.

Puntener, D., Engelke, M.F., Ruzsics, Z., Strunze, S., Wilhelm, C., and Greber, U.F. (2011). Stepwise loss of fluorescent core protein V from human adenovirus during entry into cells. J Virol *85*, 481-496.

Puntener, D., and Greber, U.F. (2009). DNA-tumor virus entry - from plasma membrane to the nucleus. Sem Cell Dev Biol *20*, 631-642.

Rabut, G., Doye, V., and Ellenberg, J. (2004). Mapping the dynamic organization of the nuclear pore complex inside single living cells. Nat Cell Biol *6*, 1114-1121.

Rao, V.B., and Feiss, M. (2008). The bacteriophage DNA packaging motor. Annu Rev Genet *42*, 647-681.

Reddy, V.S., Natchiar, S.K., Stewart, P.L., and Nemerow, G.R. (2010). Crystal structure of human adenovirus at 3.5 A resolution. Science *329*, 1071-1075.

Ribbeck, K., and Gorlich, D. (2002). The permeability barrier of nuclear pore complexes appears to operate via hydrophobic exclusion. Embo J *21*, 2664-2671.

Rietdorf, J., Ploubidou, A., Reckmann, I., Holmstrom, A., Frischknecht, F., Zettl, M., Zimmermann, T., and Way, M. (2001). Kinesin-dependent movement on microtubules precedes actin-based motility of vaccinia virus. Nat Cell Biol *3*, 992-1000.

Rux, J.J., and Burnett, R.M. (2000). Type-specific epitope locations revealed by X-ray crystallographic study of adenovirus type 5 hexon. Mol Ther *1*, 18-30.

Sargent, K.L., Meulenbroek, R.A., and Parks, R.J. (2004). Activation of adenoviral gene expression by protein IX is not required for efficient virus replication. J Virol *78*, 5032-5037.

Splinter, D., Tanenbaum, M.E., Lindqvist, A., Jaarsma, D., Flotho, A., Yu, K.L., Grigoriev, I., Engelsma, D., Haasdijk, E.D., Keijzer, N.*, et al.* (2010). Bicaudal D2, dynein, and kinesin-1 associate with nuclear pore complexes and regulate centrosome and nuclear positioning during mitotic entry. PLoS Biol *8*, e1000350.

Strawn, L.A., Shen, T., Shulga, N., Goldfarb, D.S., and Wente, S.R. (2004). Minimal nuclear pore complexes define FG repeat domains essential for transport. Nat Cell Biol *6*, 197-206.

Strunze, S., Trotman, L.C., Boucke, K., and Greber, U.F. (2005). Nuclear targeting of adenovirus type 2 requires CRM1-mediated nuclear export. Mol Biol Cell *16*, 2999-3009.

Suntharalingam, M., and Wente, S.R. (2003). Peering through the pore: nuclear pore complex structure, assembly, and function. Dev Cell *4*, 775-789.

Suomalainen, M., Nakano, M.Y., Boucke, K., Keller, S., Stidwill, R.P., and Greber, U.F. (1999). Microtubule-dependent minus and plus end-directed motilities are competing processes for nuclear targeting of adenovirus. J Cell Biol *144*, 657-672.

Suzuki, Y., and Craigie, R. (2007). The road to chromatin - nuclear entry of retroviruses. Nat Rev Microbiol *5*, 187-196.

Tang, Y., Winkler, U., Freed, E.O., Torrey, T.A., Kim, W., Li, H., Goff, S.P., and Morse, H.C., 3rd (1999). Cellular motor protein KIF-4 associates with retroviral Gag. J Virol *73*, 10508-10513.

Trotman, L.C., Mosberger, N., Fornerod, M., Stidwill, R.P., and Greber, U.F. (2001). Import of adenovirus DNA involves the nuclear pore complex receptor CAN/Nup214 and histone H1. Nature Cell Biology *3*, 1092-1100.

van Oostrum, J., and Burnett, R.M. (1985). Molecular composition of the adenovirus type 2 virion. J Virol *56*, 439-448.

Vellinga, J., Van der Heijdt, S., and Hoeben, R.C. (2005). The adenovirus capsid: major progress in minor proteins. J Gen Virol *86*, 1581-1588.

Watanabe, T.M., Yanagida, T., and Iwane, A.H. (2010). Single molecular observation of self-regulated kinesin motility. Biochemistry *49*, 4654-4661.

Wiethoff, C.M., Wodrich, H., Gerace, L., and Nemerow, G.R. (2005). Adenovirus protein VI mediates membrane disruption following capsid disassembly. J Virol *79*, 1992-2000.

Wilkins, C., and Gale, M., Jr. (2010). Recognition of viruses by cytoplasmic sensors. Curr Opin Immunol *22*, 41-47.

Wodrich, H., Cassany, A., D'Angelo, M.A., Guan, T., Nemerow, G., and Gerace, L. (2006). Adenovirus core protein pVII is translocated into the nucleus by multiple import receptor pathways. J Virol *80*, 9608-9618.

Woodward, C.L., Prakobwanakit, S., Mosessian, S., and Chow, S.A. (2009). Integrase interacts with nucleoporin NUP153 to mediate the nuclear import of human immunodeficiency virus type 1. J Virol *83*, 6522-6533.

Xue, Y., Johnson, J.S., Ornelles, D.A., Lieberman, J., and Engel, D.A. (2005). Adenovirus protein VII functions throughout early phase and interacts with cellular proteins SET and pp32. J Virol *79*, 2474-2483.

Zhang, X., Chen, S., Yoo, S., Chakrabarti, S., Zhang, T., Ke, T., Oberti, C., Yong, S.L., Fang, F., Li, L.*, et al.* (2008). Mutation in nuclear pore component NUP155 leads to atrial fibrillation and early sudden cardiac death. Cell *135*, 1017-1027.

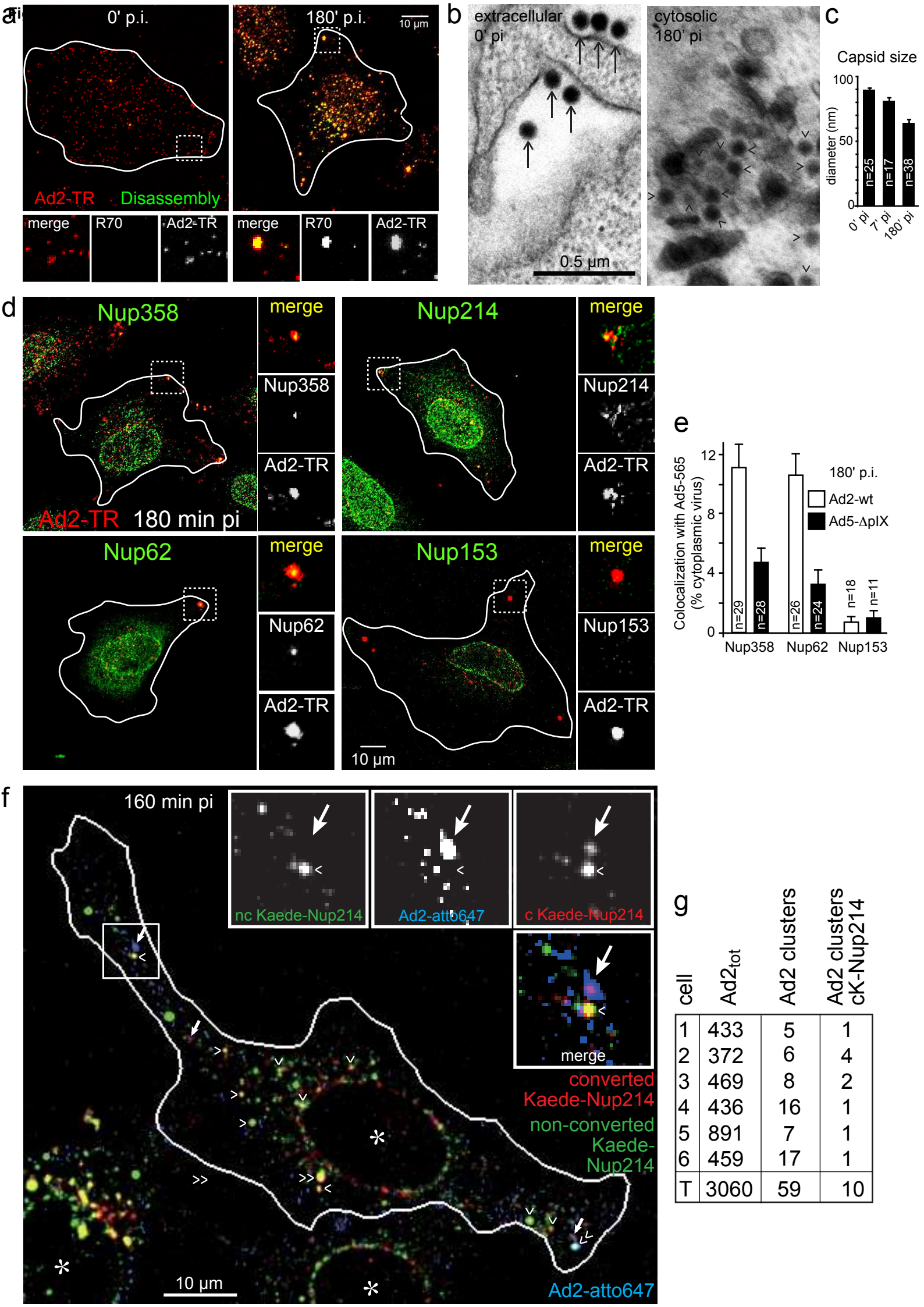

g

cell	$Ad2_{tot}$	Ad2 clusters	Ad2 clusters cK-Nup214
1	433	5	1
2	372	6	4
3	469	8	2
4	436	16	1
5	891	7	1
6	459	17	1
T	3060	59	10

Figure2

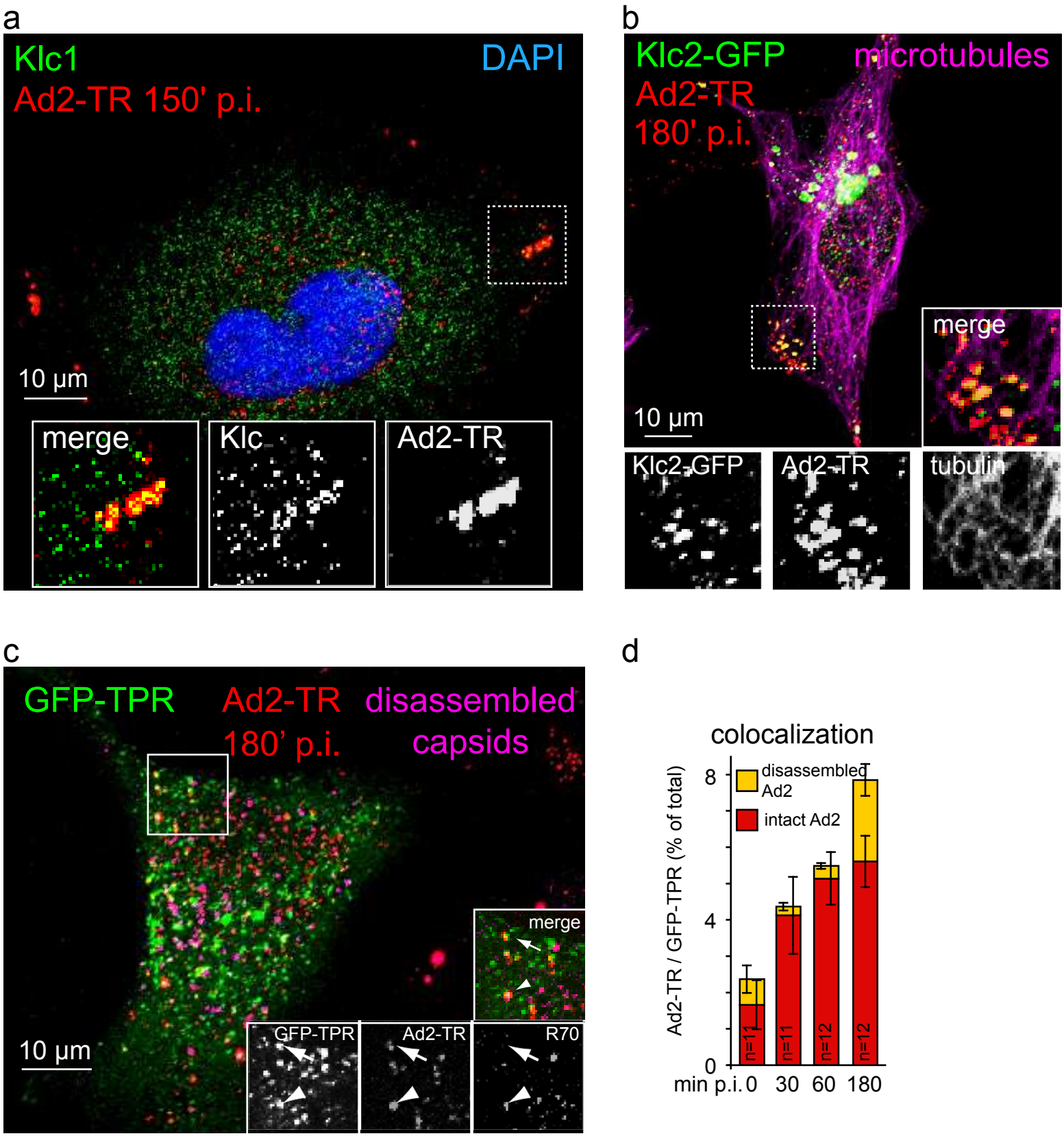
a
Klc1
Ad2-TR 150' p.i.
DAPI
10 µm
merge
Klc
Ad2-TR
b
Klc2-GFP
Ad2-TR
180' p.i.
microtubules
merge
10 µm
Klc2-GFP
Ad2-TR
tubulin
c
GFP-TPR
Ad2-TR
180' p.i.
disassembled capsids
merge
10 µm
GFP-TPR
Ad2-TR
R70
d
colocalization
Ad2-TR / GFP-TPR (% of total)
disassembled Ad2
intact Ad2
min p.i. 0 30 60 180
n=11
n=11
n=12
n=12
e
disassembly
disassembled virus (R70, AU)
0' p.i.
180' p.i.
n=16
n=16
n=16
n=15
GFP
GFP-TPR
f
infection
Ad2-mRFP (relative fluorescence)
n=56
n=56
GFP
GFP-TPR
g
infection
Klc interference
Ad2-mRFP (arbitrary units)
siRNA
n.sil.
Klc1
h
infection
Khc interference
Ad2-mRFP (arbitrary units)
siRNA
n.sil.
Kif5B
Kif5C
i
disassembly
disassembled Ad2 (R70, AU)
0' p.i.
180' p.i.
n = 54
n = 60
n = 47
n = 39
siRNA
n.sil.
Klc1
Kif5C

Figure3

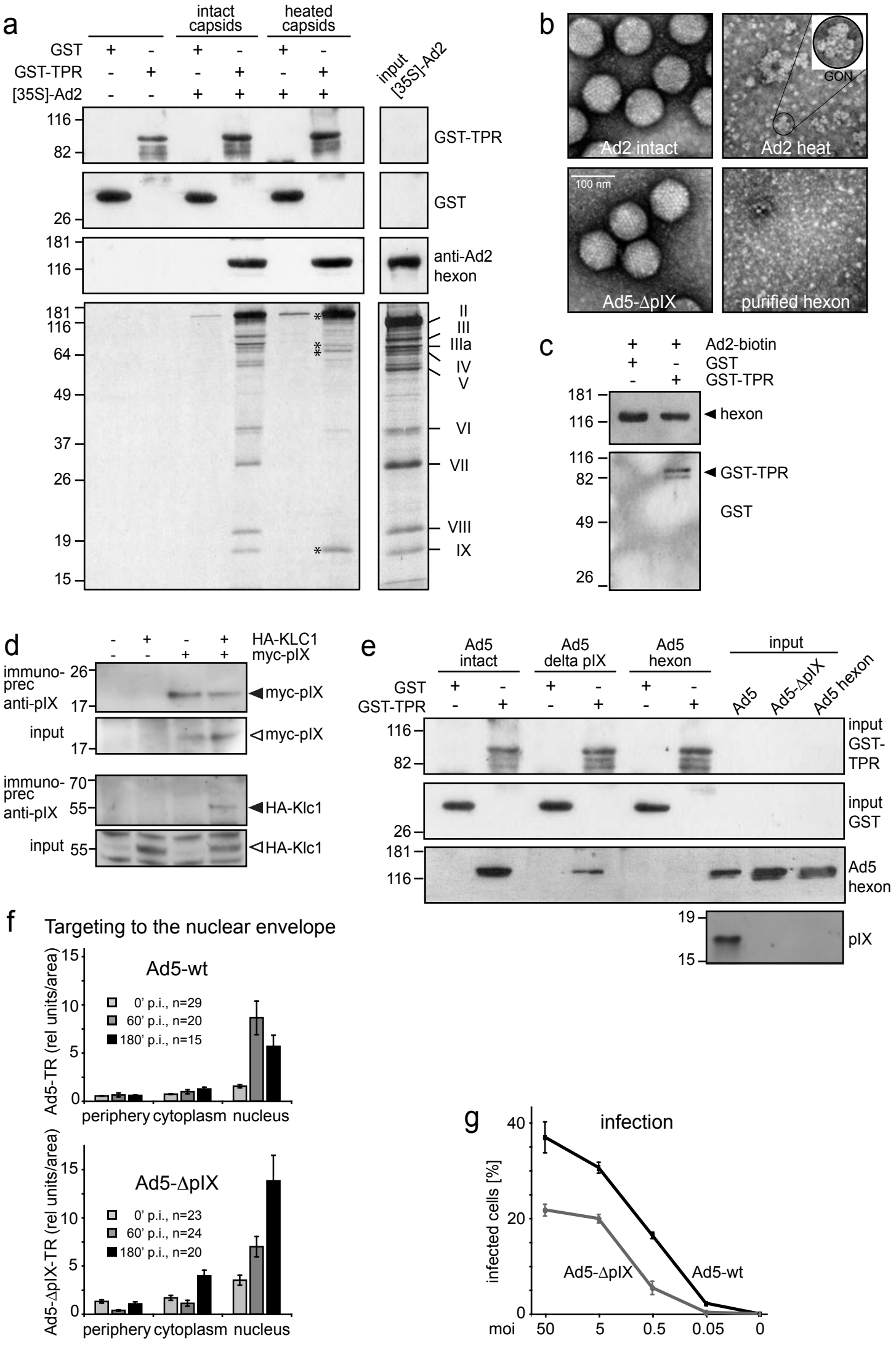
a
intact capsids
heated capsids
GST
GST-TPR
[35S]-Ad2
input [35S]-Ad2
GST-TPR
GST
anti-Ad2 hexon
II
III
IIIa
IV
V
VI
VII
VIII
IX
b
Ad2 intact
Ad2 heat
GON
100 nm
Ad5-ΔpIX
purified hexon
c
Ad2-biotin
GST
GST-TPR
hexon
GST-TPR
GST
d
HA-KLC1
myc-pIX
immuno-prec anti-pIX
input
myc-pIX
HA-Klc1
e
Ad5 intact
Ad5 delta pIX
Ad5 hexon
input
Ad5
Ad5-ΔpIX
Ad5 hexon
input GST-TPR
input GST
Ad5 hexon
pIX
f
Targeting to the nuclear envelope
Ad5-wt
0' p.i., n=29
60' p.i., n=20
180' p.i., n=15
Ad5-TR (rel units/area)
periphery cytoplasm nucleus
Ad5-ΔpIX
0' p.i., n=23
60' p.i., n=24
180' p.i., n=20
Ad5-ΔpIX-TR (rel units/area)
periphery cytoplasm nucleus
g
infection
infected cells [%]
Ad5-ΔpIX
Ad5-wt
moi 50 5 0.5 0.05 0

Figure4

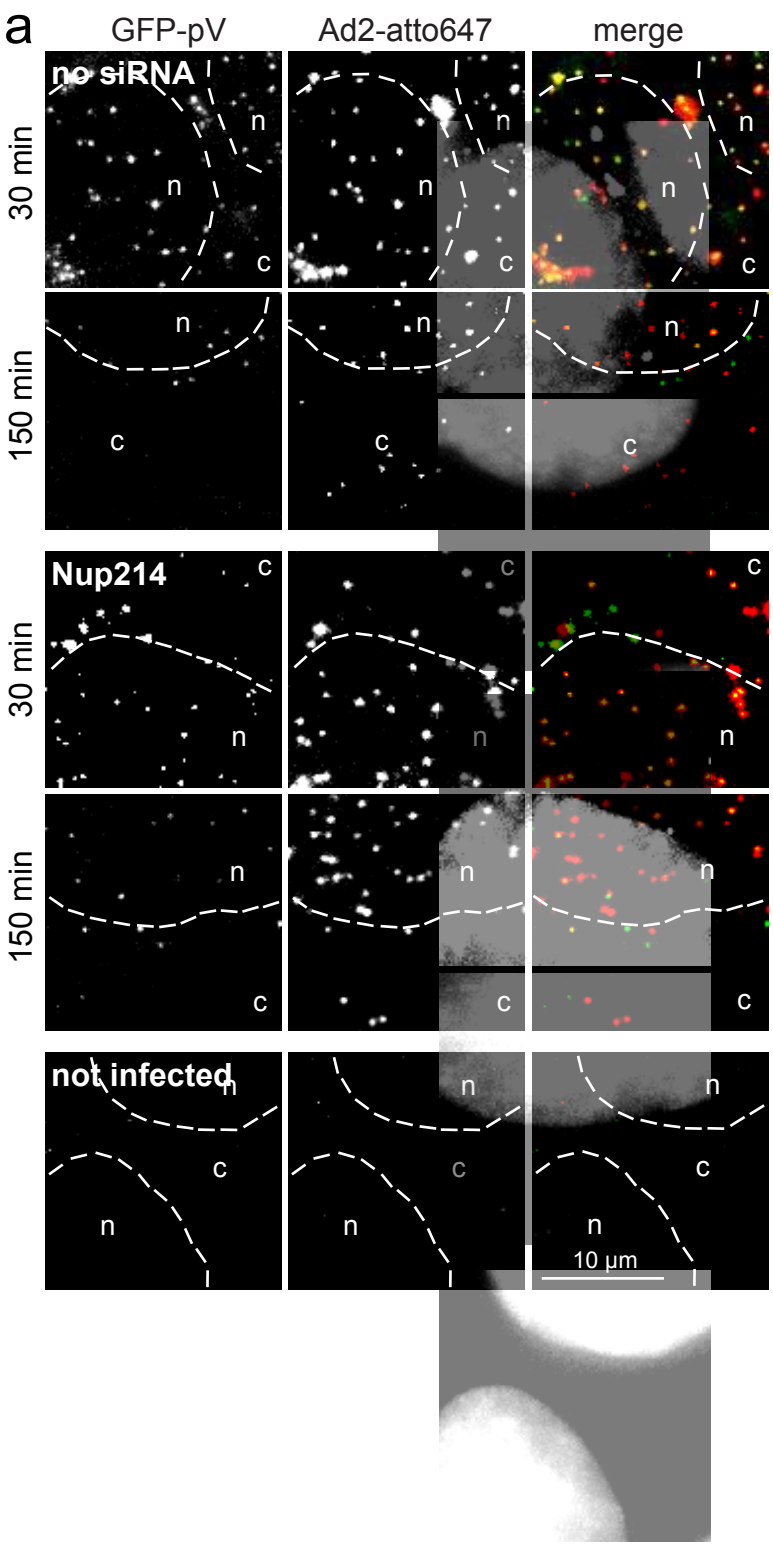

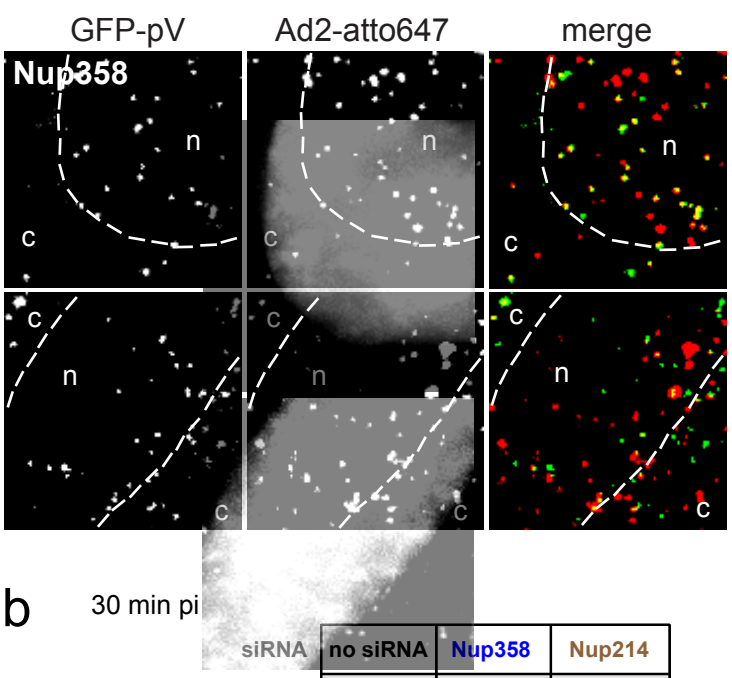

b

30 min pi

siRNA	no siRNA	Nup358	Nup214
GFP-pV / Ad2-atto647	1	1	1
standard error	0.0169	0.0170	0.0250
n	8	9	7
viruses (*1000)	28	31	22
cells	480	540	420

150 min pi

siRNA	no siRNA	Nup358	Nup214
GFP-pV / Ad2-atto647	0.6780	0.9647*	0.8233°
standard error	0.0275	0.0242	0.0340
n	9	8	9
viruses (*1000)	31	21	28
cells	540	480	540

* p = 1.14E-6 ° p = 0.0045

Figure5

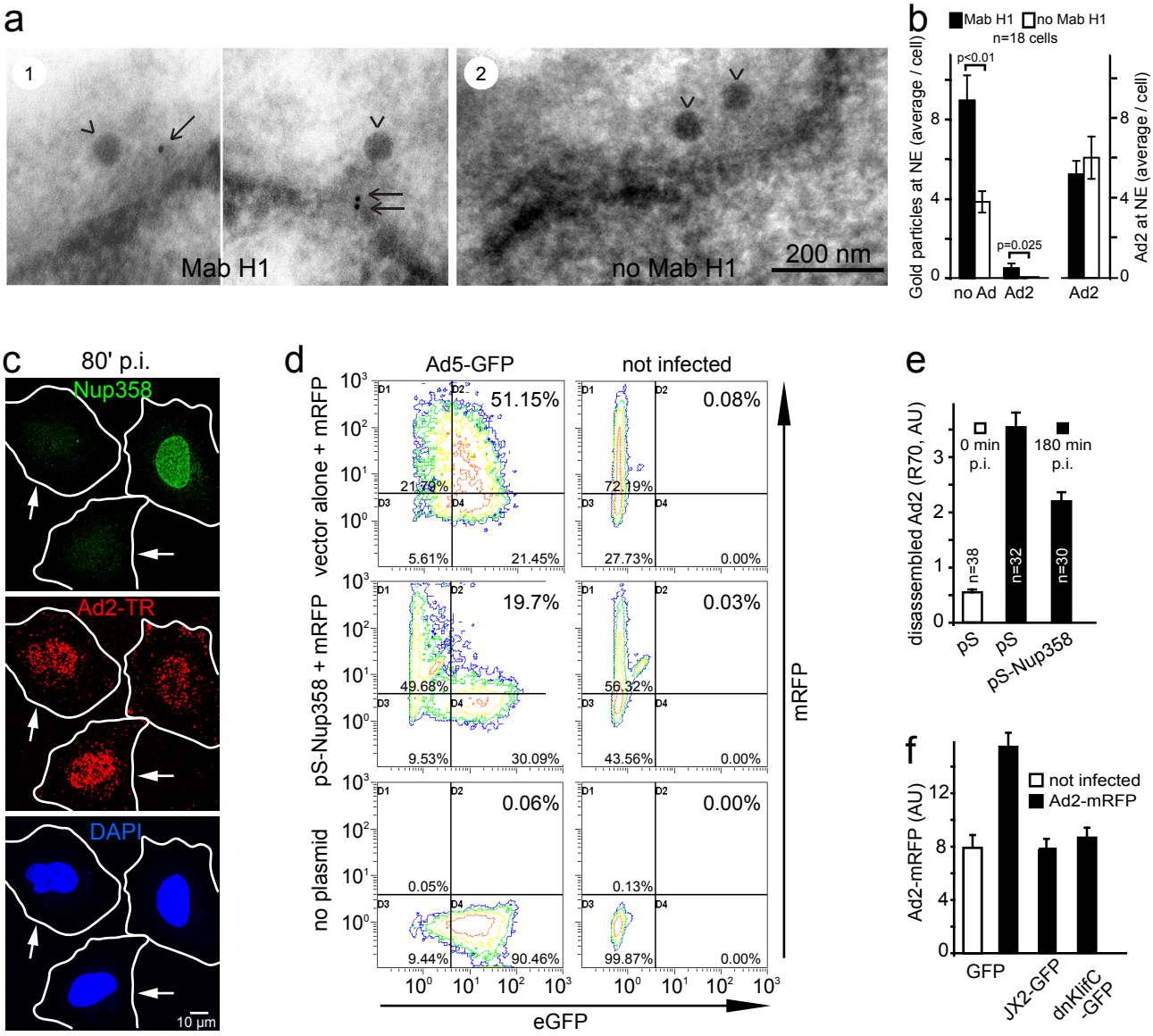
a
1
2
Mab H1
no Mab H1
200 nm
b
Mab H1
no Mab H1
n=18 cells
p<0.01
p=0.025
Gold particles at NE (average / cell)
Ad2 at NE (average / cell)
no Ad
Ad2
Ad2
c
80' p.i.
Nup358
Ad2-TR
DAPI
10 µm
d
Ad5-GFP
not infected
vector alone + mRFP
pS-Nup358 + mRFP
no plasmid
51.15%
0.08%
21.79%
72.19%
5.61%
21.45%
27.73%
0.00%
19.7%
0.03%
49.68%
56.32%
9.53%
30.09%
43.56%
0.00%
0.06%
0.00%
0.05%
0.13%
9.44%
90.46%
99.87%
0.00%
mRFP
eGFP
e
disassembled Ad2 (R70, AU)
0 min p.i.
180 min p.i.
n=38
n=32
n=30
pS
pS
pS-Nup358
f
Ad2-mRFP (AU)
not infected
Ad2-mRFP
GFP
JX2-GFP
dnKifC -GFP

Figure6

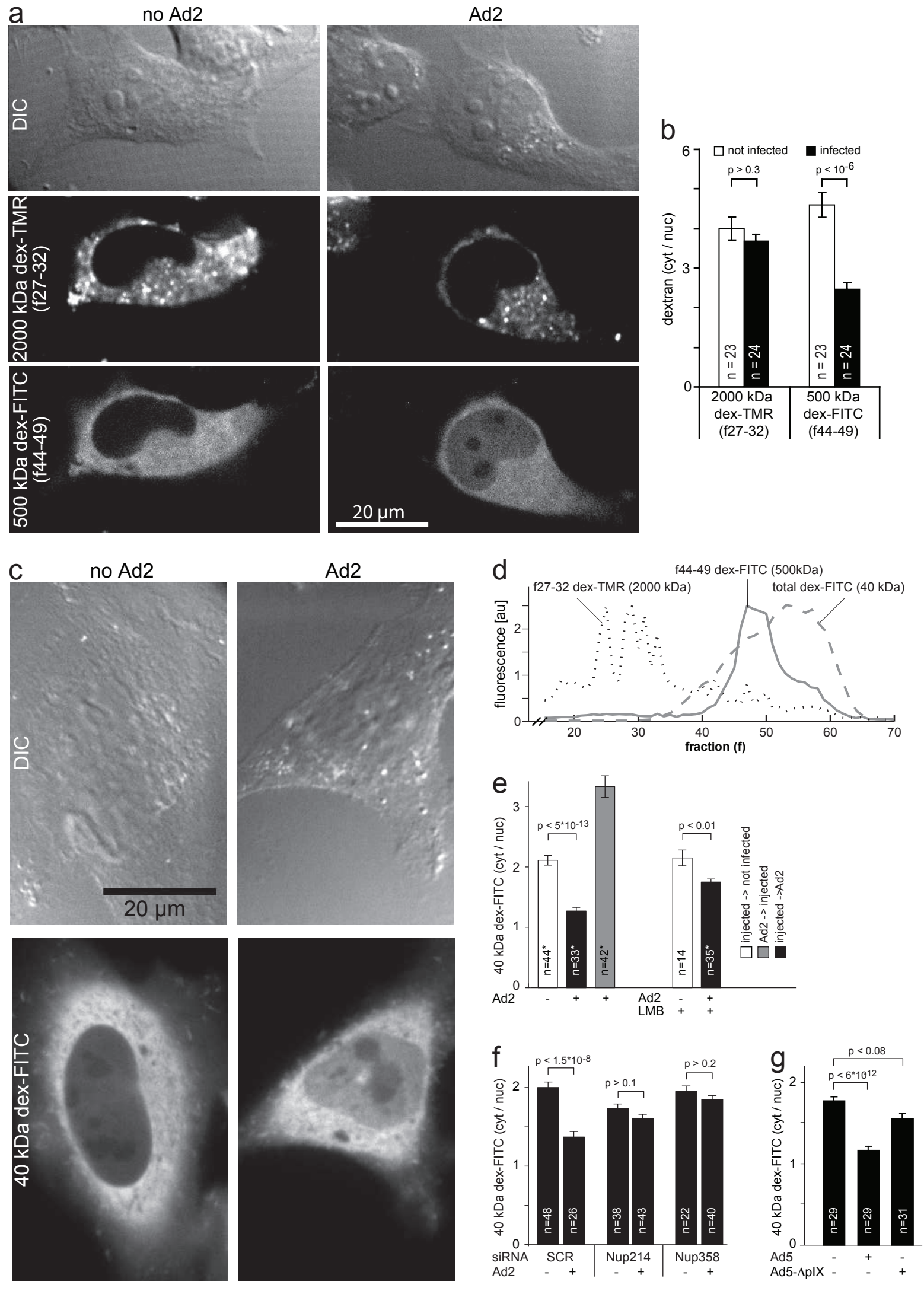
a
no Ad2
Ad2
DIC
2000 kDa dex-TMR (f27-32)
500 kDa dex-FITC (f44-49)
20 µm
b
not infected
infected
p > 0.3
p < 10-6
dextran (cyt / nuc)
n = 23
n = 24
n = 23
n = 24
2000 kDa dex-TMR (f27-32)
500 kDa dex-FITC (f44-49)
c
no Ad2
Ad2
DIC
20 µm
40 kDa dex-FITC
d
f44-49 dex-FITC (500kDa)
f27-32 dex-TMR (2000 kDa)
total dex-FITC (40 kDa)
fluorescence [au]
fraction (f)
e
p < 5*10-13
p < 0.01
40 kDa dex-FITC (cyt / nuc)
n=44*
n=33*
n=42*
n=14
n=35*
injected -> not infected
Ad2 -> injected
injected ->Ad2
Ad2
Ad2
LMB
f
p < 1.5*10-8
p > 0.1
p > 0.2
40 kDa dex-FITC (cyt / nuc)
n=48
n=26
n=38
n=43
n=22
n=40
siRNA
SCR
Nup214
Nup358
Ad2
g
p < 0.08
p < 6*1012
40 kDa dex-FITC (cyt / nuc)
n=29
n=29
n=31
Ad5
Ad5-ΔpIX

Figure7

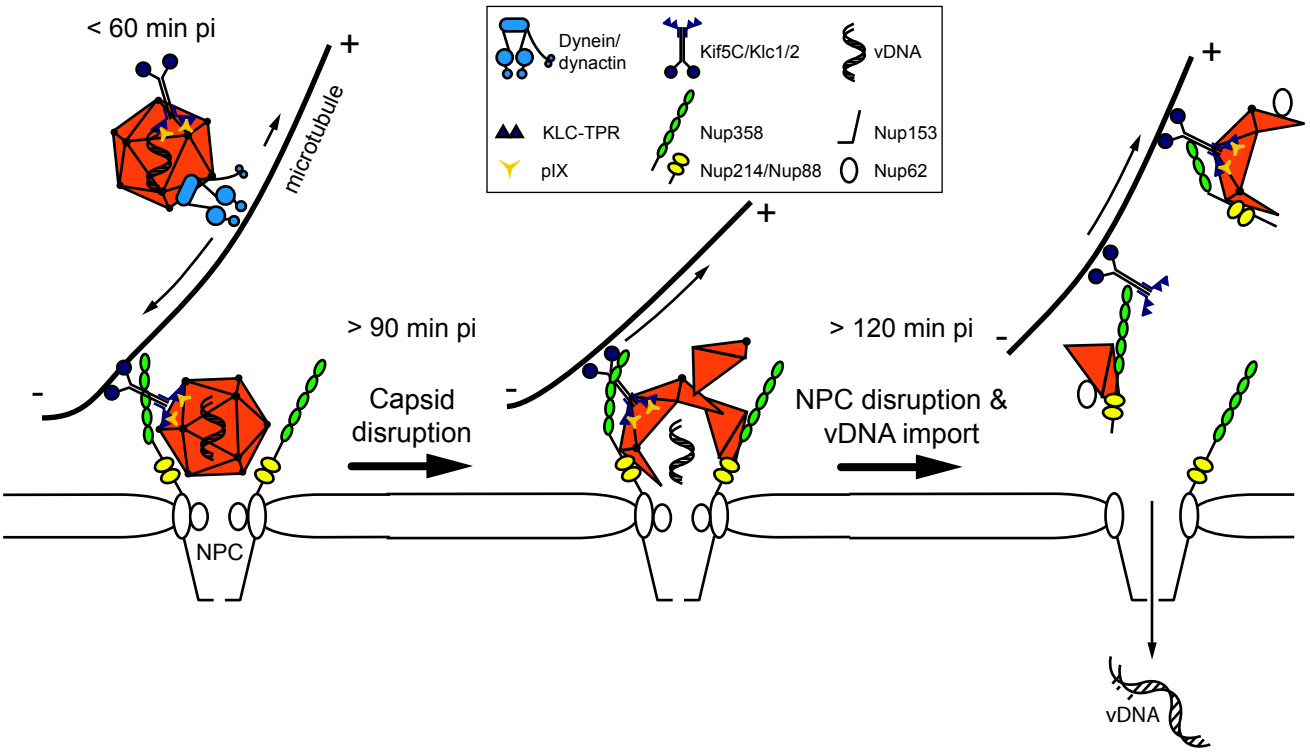
< 60 min pi
microtubule
+
-
Dynein/
dynactin
Kif5C/Klc1/2
vDNA
KLC-TPR
Nup358
Nup153
pIX
Nup214/Nup88
Nup62
> 90 min pi
Capsid
disruption
> 120 min pi
NPC disruption &
vDNA import
NPC
vDNA

Inventory of Supplemental Information

TABLE OF CONTENTS

SUPPLEMENTAL INFORMATION

Supplemental Data

Supplemental Fig. S1: Characterization of adenovirus uncoating (related to Fig. 1).

A) Predominant reactivity of the anti-hexon antibody R70 with broken Ad2 capsids, and visualization of Ad2 capsid remnants in the cell periphery (related to Fig. 1a and b)

a) Purified intact Ad2 (0.1 mg/ml) or heat disrupted Ad2 particles (56°C for 10 min) were desposited on glow discharged EM grids and incubated with or without R70 (5 µg/ml) for 30 min, followed by staining with secondary goat anti-rabbit IgG coupled to 10 nm colloidal gold (0.2 µg/ml, BBI International) for 30 min at room temperature. Images were recorded in a Zeiss TEM-10, typically at 50'000 magnification, 80 kV. White arrows depict intact Ad2 capsids, black arrows disrupted capsids, and arrowheads point out gold particles on disrupted (white) or heat denatured capsids (black).

b) HeLa cells grown on indexed glass coverslips were infected with Ad2-Texas red (TR) for 180 min, fixed with 3% para-formaldehyde and 0.1% glutaraldehyde, and imaged by differential interference microscopy (1) and fluorescence microscopy (2). Insets show magnified views of an area containing virus clusters. The cells were then prepared for thin section transmission electron microscopy, verified by phase contrast microscopy (3) and imaged at low and high magnifications (4). The boxed area in (4) highlighted with an arrow contains a cluster of cytosolic viral capsid fragments.

B) No localization of Nup358 with Ad5ΔpIX-atto565, or Nup358, Nup214, Nup153, Nup62, or RanGAP and Crm1 in the periphery of non-infected or LMB-treated infected cells (related to Fig. 1d)

a,b) HeLa cells were infected with Ad5-atto565 or Ad5ΔpIX-atto565 for 180 min, fixed, immune-stained for Nup358 and analysed by confocal fluorescence microscopy. Note that there is little colocalization of Ad5ΔpIX-atto565 with cytoplasmic Nup358. Boxed areas show enlarged regions from the cell periphery.

c-e) Cycloheximide-treated HeLa cells were either not infected or infected with Ad2-TR for 180 min, or treated with leptomycin B (LMB, 20 nM) and infected, fixed, immune-stained for nucleoporins, RanGAP1 or Crm1, and analysed by single section confocal laser scanning microscopy through the lower region of the cells as described in the main text.

C) Displacement of nucleoporins and Crm1-GFP from the nuclear envelope to the cell periphery in Ad2 infected cells (related to Fig. 1d).

Still images of periphery-directed Ad2-atto565 co-localizing with Crm1-GFP 150 min pi. One particular virus particle was followed over 36.4 sec during its trajectory of about 30 µm from the nuclear envelope to the cell periphery (box). The complete frames of this experiment are available in Suppl. Mov. 1.

D) Kaede-Nup214 localizes to the nuclear envelope in non-infected cells, and analyses by a custom-made algorithm to detect clustered Ad2 particles in the cytoplasm (related to Fig. 1f)

a) HeLa cells transfected with Kaede-Nup214 for 24 h were imaged before photo-conversion (top row), and after photo-conversion of the nuclear area (marked by star *, lower row). Note the non-converted Kaede-Nup214 (green) in the nuclear envelope, and the absence of photo-converted Kaede-Nup214 (red) before conversion. Also note the appearance of red fluorescent Kaede-Nup214 after conversion. A cytoplasmic aggregate of Kaede-Nup214 gave fluorescent green and red signals independent of conversion (arrow head). Another aggregate of green fluorescent Kaede-Nup214 outside the photo-converted nuclear area had no

red fluorescence at all (arrow) confirming the high degree of specificity of photo-conversion.

b) Performance of an algorithm to detect regular shaped and clustered Ad2-atto647 particles, based on DIC image, maximum projection of confocal stacks of Ad2-atto647, color coded regular particles (green), clustered particles (white), and particles from other cells not analysed, and a histogram of all particles detected.

Supplemental Figure S1

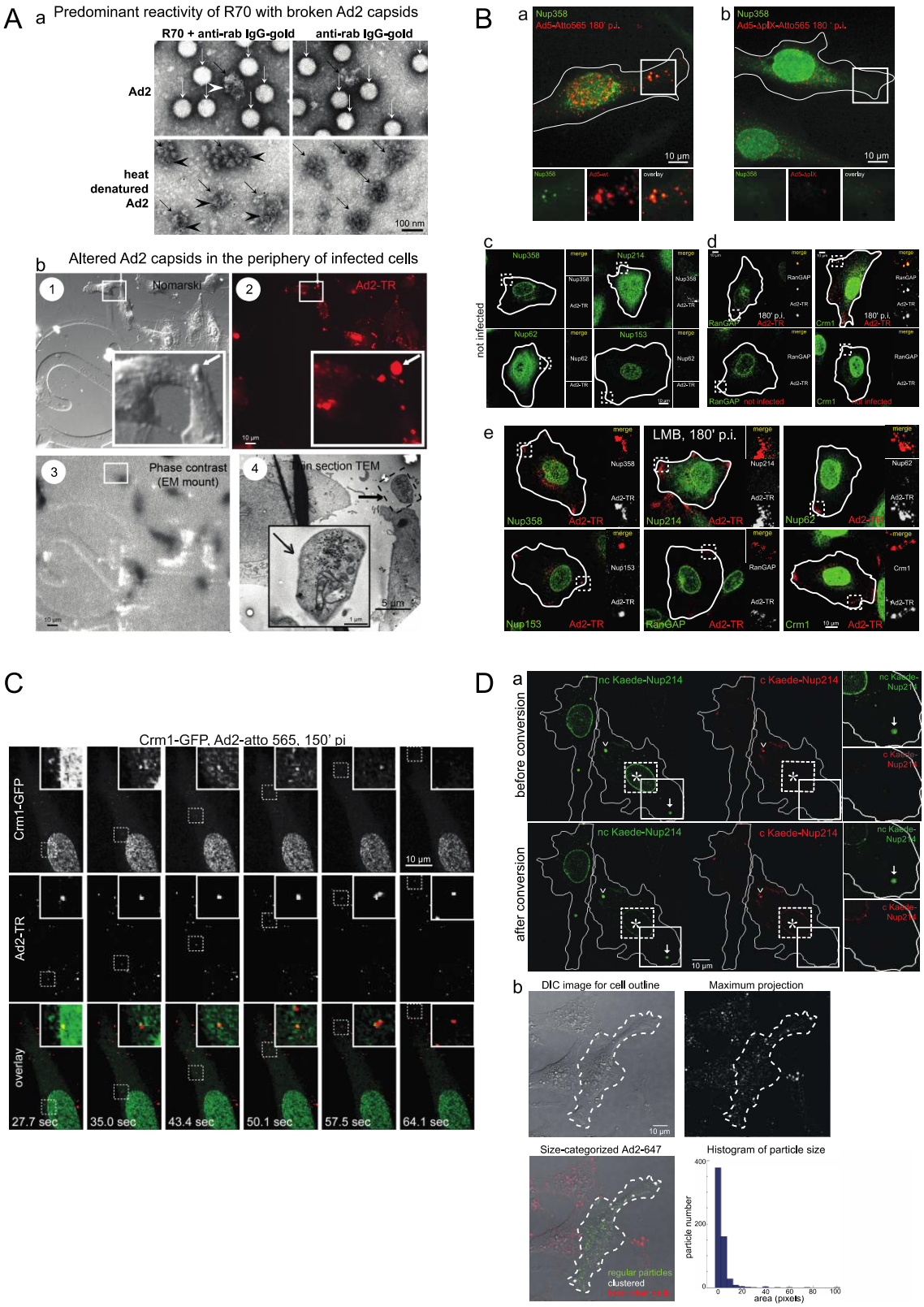

Supplemental Fig. S2: Adenovirus trafficking to the nucleus is independent of kinesin-1 (related to Fig. 2).

A) Nuclear targeting of incoming adenovirus is independent of kinesin-1 but dependent on the dynactin protein p50/dynamitin (related to Fig. 2a-d).

a-c) HeLa cells expressing GFP-TPR, GFP or p50/dynamitin-GFP (p50-GFP) were infected with Ad2-TR as indicated, fixed and analysed by CLSM. Ad2-associated fluorescence was quantified in the cell periphery (outer most 3.5 µm), the cytoplasm (total cell area excluding the peripheral and nuclear areas), and over the nucleus as described earlier (Nakano and Greber, 2000). Note that GFP-TPR did not affect the transport of Ad2-TR to the nucleus, unlike p50-GFP which is a dynein/dynactin inhibitor, and blocks microtubule-dependent transport of Ad2 to the nucleus (Burkhardt et al., 1997; Suomalainen et al., 1999). Importantly, GFP-TPR decreased the levels of virus particles in the periphery 180 min pi, compared to GFP or p50/dynamitin expressing cells, suggesting that the transport of Ad2-TR fragments to the cell periphery requires kinesin-1.

d) GFP-TPR does not affect endosomal escape of virus particles (v.p.) as indicated by quantitative thin section electron microscopy.

e) p50-GFP inhibits Ad2-mRFP in agreement with the notion that dynein/dynactin is required for transport of Ad2 to the nucleus (Suomalainen et al., 1999).

B) siRNAs against kinesin-1 specifically knock down their target mRNAs, but do not affect endosomal escape of Ad2 (related to Fig. 2g-i).

a,b) HeLa cells were transfected with siRNAs targeting the kinesin light chains Klc1 or Klc2 (A), or the heavy chain Kif5B or Kif5C. Knockdown was quantified by SYBR-green real time PCR on isolated cellular RNA using specific primers. Fold changes of triplicate measurements of mRNA levels including standard deviations are shown.

c) Subcellular analyses of Ad2 localization from thin section electron micrographs 60 min pi show that siRNAs against Klc1 or Kif5C or non-silencing (n.s.) siRNAs have no significant effects on viral endocytosis or escape from endosomes to the cytosol.

Supplemental Figure S2

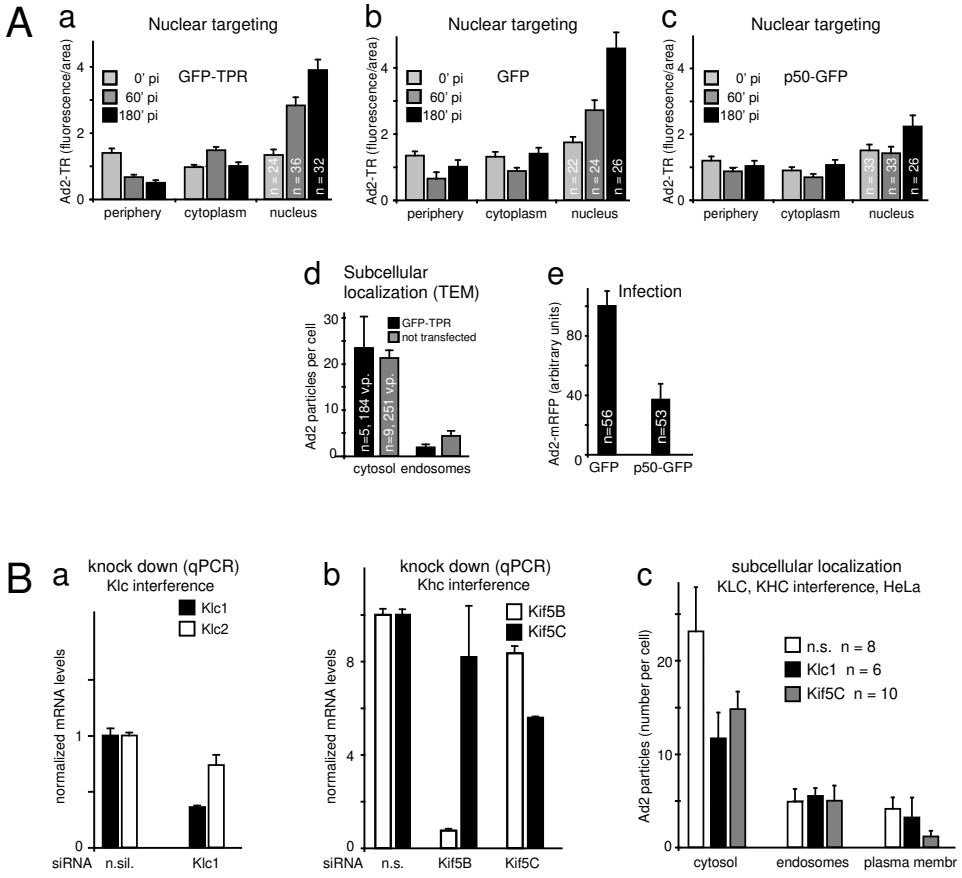

Supplemental Fig. S3: Nup214 is required for nuclear localization of adenovirus (related to Fig. 4).

a, b) HeLa cells were transfected with pSuper plasmids encoding shRNAs against Nup214, Nup358 or empty plasmid together with an eGFP-encoding transfection marker plasmid for 24 h, or were treated with or wthout 40 µM nocodazole for 30 min, and then infected with Ad2-atto565 for 90 min upon cold synchronization (A). Cells were fixed and analysed for subcellular localization of Ad2-atto565 as described in supplemental experimental procedures.

c-e) Knock-down analyses of cells treated with siRNA against Nup214 or Nup358 by indirect immune-fluorescence microscopy, and quantification of the nuclear signals with number of cells and estimated knock-down efficiencies.

Supplemental Figure S3

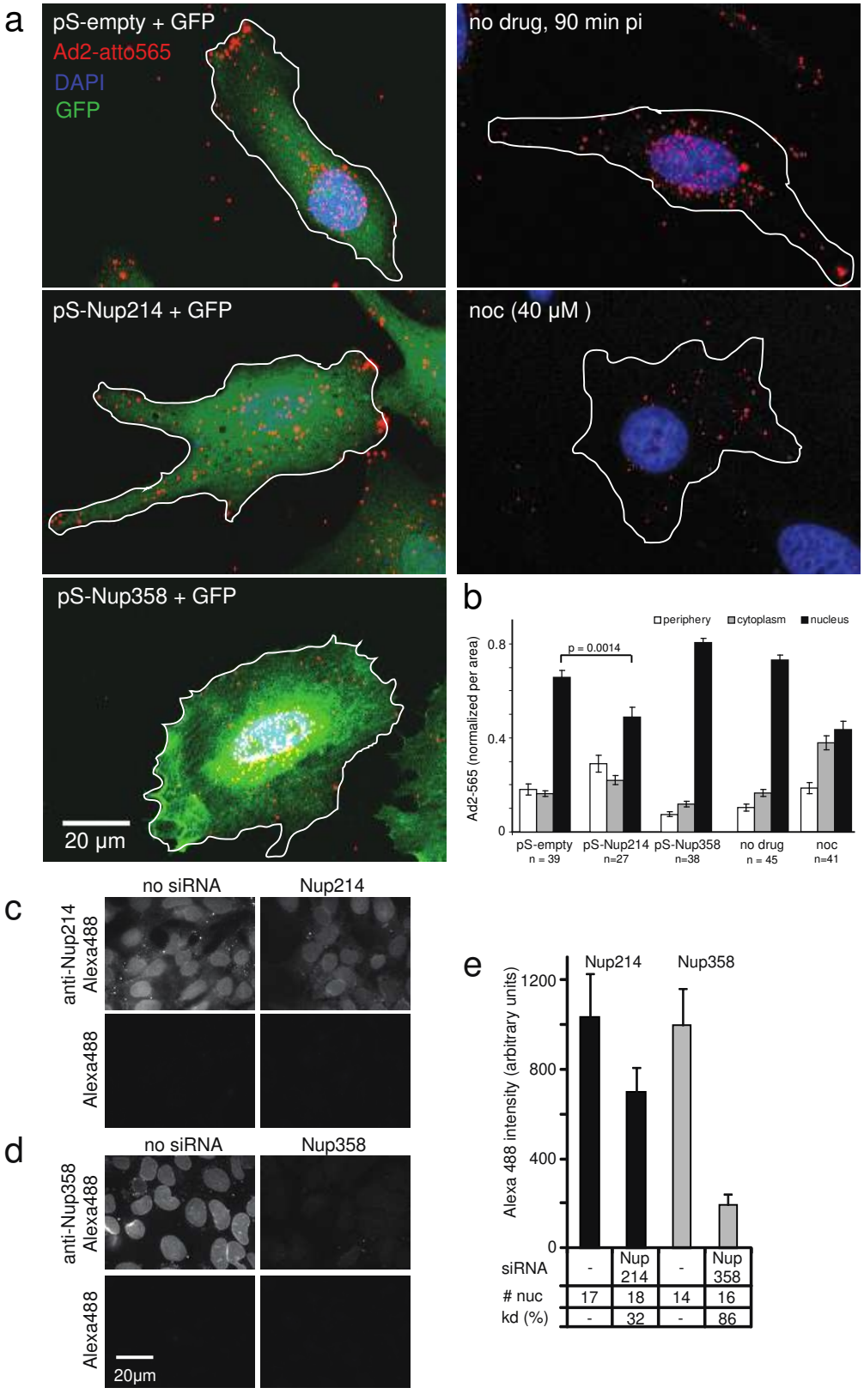

Supplemental Fig. S4: Knock-down of Nup358 inhibits Ad5 but not HSV1 infection (related to Fig. 5C).

HeLa cells transfected with mRFP, pS (empty vector) or pS-Nup358 were infected with Ad5-GFP or HSV1-GFP for 6 or 9 h at moi 5, fixed and analysed for infected cells.

a) Exemplary fields 9 h pi with magnified views of boxed areas with DAPI, mRFP, GFP and merged mRFP plus GFP (two columns on the right side).

b) Quantitative infection analysis of RFP-positive cells, including number of cells analysed (n) at 6 and 9 h pi.

Supplemental Figure S4

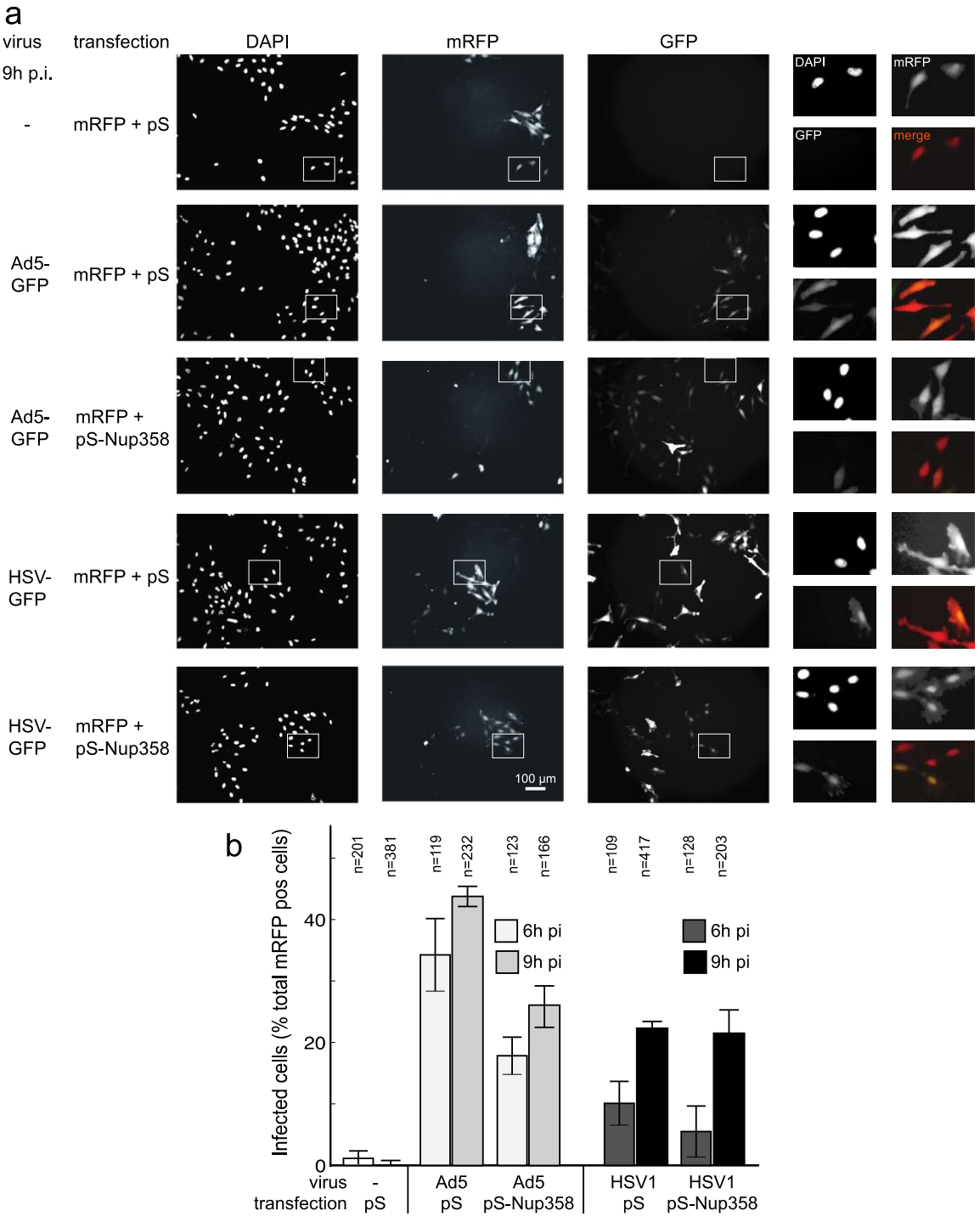

Supplemental Movie S1: Dynamic colocalization of Crm1-GFP with incoming Ad2-atto565 (related to Fig. 1d).

HeLa cells expressing Crm1-GFP were infected with Ad2-565 for 150 min, and imaged by spinning disc confocal microscopy in beam splitter mode with simultaneous acquisition of both channels. Acquisition frequency 6.7 Hz.

Supplemental Movie S1

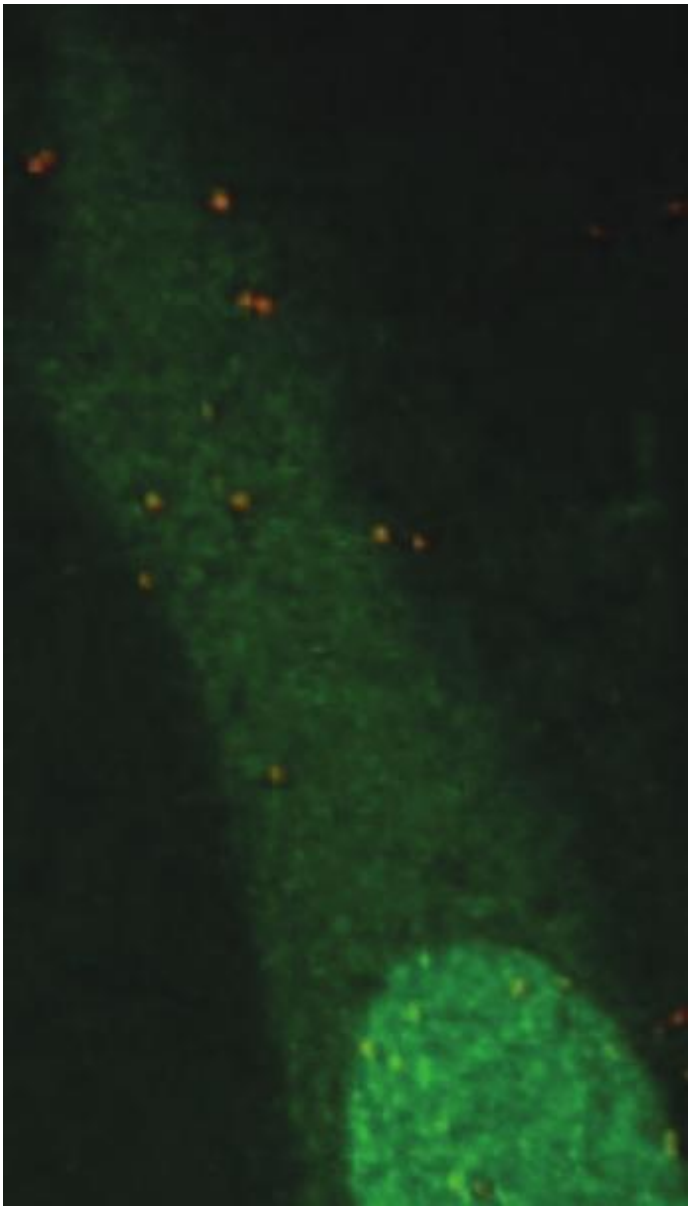

Supplemental Movie S2: High levels of dynamic colocalization of Klc2-GFP with incoming Ad2-565 after viral disassembly (related to Fig. 2b).

HeLa cells expressing Klc2-GFP were infected with Ad2-565 for 239 min, and imaged by spinning disc confocal microscopy in beam splitter mode with simultaneous acquisition of both channels. Acquisition frequency was 4 Hz.

Supplemental Movie S2

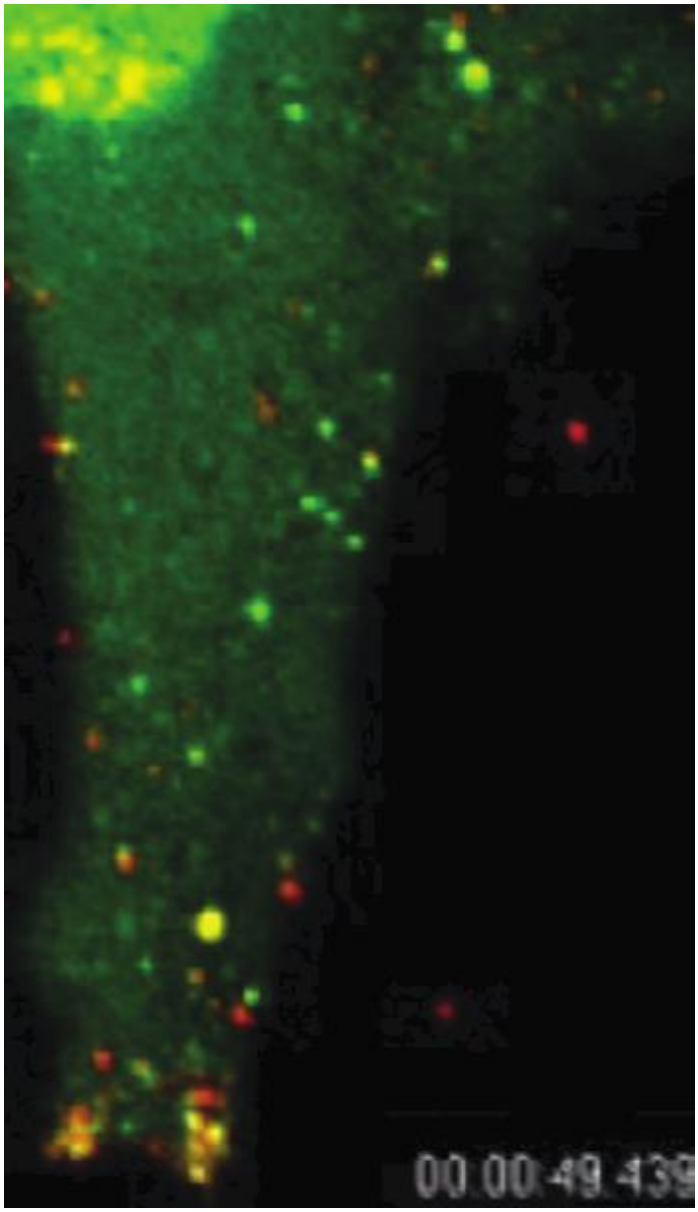

Supplemental Experimental Procedures

Cells

HeLa cells were obtained from Dr. U. Kutay (Swiss Federal Institute of Technology Zurich, Switzerland), KB and HEK293T cells were purchased from the American Type Culture Collection, human embryonic retinoblast 911 cells were from Dr. S. Hemmi (University of Zurich, Switzerland). Cells were grown in Dulbecco's modified Eagle's medium supplemented with 10 % fetal bovine serum and 1% nonessential amino acids (Gibco-BRL).

Viruses

Ad2 and Ad5 were grown, isolated and labeled with TR or atto565 (Atto-TEC, Siegen, Germany) as described before (Suomalainen et al., 1999). [^{35}S]-methionine-labeled Ad2 ([^{35}S]-Ad2) was prepared in 10^8 KB cells using 1 mCi of RedivuePRO-MIX (Amersham Biosciences) as published (Greber et al., 1993). Heat disrupted Ad2 was prepared as described (Russell et al., 1967). Transgenic Ad2-mRFP was generated by ET recombination mediated insertion of a mRFP expression cassette (Imelli et al., 2009). Homologous sequences targeted the CMV promotor driven expression cassette to the E1 region of Ad2 (nucleotides 461-3510). BAC-DNA was verified for correct insertion of the mRFP gene (Giepmans et al., 2006), purified and transfected into Ad5-E1 expressing human embryonic retinoblast 911 cells. Three sequential rounds of infection were used to produce purified viruses. Transgenic Ad5-ΔpIX (Ad5 dl313, provided by R. Hoeben, Leiden University Medical Center, The Netherlands), and Ad5-GFP and Ad2-mRFP were grown in the E1 complementing cell line human embryonic retinoblast 911 (Vellinga et al., 2005). Infections of HeLa cells were carried out as described (Suomalainen et al., 1999; Trotman et al., 2001), or further specified in supplemental materials. Atto647-labelled Ad2-GFP-pV was prepared as described

(Puntener et al., 2011). Recombinant proteins, protein pull-downs and co-immune-precipitations are described in supplemental materials.

Antibodies and chemicals

Rabbit anti-hexon R70 and anti-fiber and penton R73 antibodies were used as described (Trotman et al., 2001). Rabbit anti-proteins IX antibodies were from M. Rosa-Calatrava (Virologie et de Pathogénèse Virale, RTH Laennec, Lyon, France, Rosa-Calatrava et al., 2001). Monoclonal antibodies L1 against Klc (Mab1613) and H1 against kinesin heavy chain (Khc) (Mab1616) were from Chemicon International as described (Pfister et al., 1989). The H1 antibody recognizes recombinant Kif5A and Kif5C but not Kif5B (Cai et al., 2001). Antibodies against the C-terminus of Nup214, and Crm1 were from M. Fornerod (Fornerod et al., 1997), against Nup358 from F. Melchior (Department of Biochemistry, University of Gottingen, Germany, Hutten et al., 2008), and Mab SA1 against the carboxy-terminus of Nup153 was from B. Burke (University of Florida College of Medicine, Bodoor et al., 1999). Monoclonal anti-HA (clone HA-7) was purchased from Sigma, anti-c-myc (clone 9E10) from Santa Cruz Biotechnology. Goat antibodies against mouse or rabbit IgG coupled to horseradish peroxidase were from Sigma (Sigma Chemical Co., St. Louis, MO), against mouse or rabbit IgG coupled to Alexa 488 or 594 from Molecular Probes (Leiden, The Netherlands) and antibodies coupled to Cy5 from Jackson Immuno Research (West Grove, PA). DAPI was used as indicated by the manufacturer (Molecular Probes).

RNA interference

siRNAs (Qiagen) and pSUPER plasmid encoding Nup358 shRNA (Bernad et al., 2004) were transfected with Lipofectamin2000/Opti-MEM (Invitrogen), or electroporation, respectively. Specifically, 25 µl Opti-MEM containing 40 nM siRNA (final concentration) against Nup358 (5'-CGA GGU CAA UGG CAA ACU ATT-3')

or Nup214 (5'-UUG CCC AAG GAA CGC UCG ATT-3') or no siRNA and 0.125 ul Lipofectamin was added to a 96-well clear bottom plate. HER-911 cells in 75 µl DMEM/10% FBS/1% NEA/1% PS were added to 30% confluency and incubated for 3 days at 37°C and 5% CO_2. For background controls medium was added to wells containing no cells.

Kinesin-1 targeting siRNAs (Kif5B sense: GACCAACCTTTCAGTTCA·d(TT), Kif5C sense: CTTGGCTGTTCATGAAGAT·d(TT), Klc1 sense: AAGCATCTGGAGTTTATGAAT·d(TT), Klc2 sense AGAGTTTGGCTCTGTCAAT·d(TT), Klc3: Cat. No. SI02776557) and non-silencing control siRNA were obtained from Qiagen. HeLa cells were transfected with 50 pmol siRNA at a confluency of 70% in 6-well dishes using Lipofectamine 2000 and Opti-MEM reduced serum medium (Invitrogen). After 48 hours, cells were subjected to a second transfection and subjected to further experimentation at 96 h post first transfection. To analyse the gene knockdown by real-time RT-PCR, $4x10^5$ cells were harvested, lysed and cellular RNA was isolated using the NucleoSpin RNA II kit according to the manufactures protocol (Macherey-Nagel AG, Switzerland). DNase I treatment removed contaminating DNA. For the first strand cDNA synthesis, 300 ng purified RNA were used as template and reverse transcribed using the SuperScript III Platinum Two-Step qRT-PCR Kit (Invitrogen) followed by a RNase H treatment to remove template RNA. Triplicates of SYBR-green real-time PCR were performed using gene specific primers. Results were normalized to the mean of three housekeeping genes and expressed as fold changes of gene-specific mRNA levels including the standard error of the mean (SEM). To knockdown Nup358, plasmid DNA encoding shRNAs were kindly provided by M. Fornerod (Bernad et al., 2004). HeLa cells were co-transfected with pSuper-Nup358 and mRFP encoding plasmids by electroporation and analysed for knockdown at 84h post transfection.

cDNAs and transfections

GFP-TPR, GST-TPR and Klc2-GFP expressing constructs were used as described (Newsome et al., 2004). HA-Klc1 was obtained from P. Sonderegger (University of Zurich, Switzerland), CRM1-GFP from M. Fornerod (The Netherlands Cancer Institute, Amsterdam), Nup214-GFP from J. Ellenberg (EMBL, Heidelberg, Germany) and YFP-RanGAP1 from F. Melchior (Department of Biochemistry, University of Heidelberg, Germany). p50/dynamitin (Burkhardt et al., 1997) was fused to eGFP and expressed from the pcDNA3 vector under the CMV promotor in Fugene6 transfected cells. Myc-pIX encoding plasmid DNA was constructed by PCR using the synthetic oligonucleotides CGCGAATTCGGAGCACCAACTCGTTTGAT as 5'-terminal and CCCCTCCGATTAAACCGCATTGGGAGG as 3'-terminal primers for the amplification of the pIX gene from genomic DNA of human Ad5, and subsequent ligation into EcoRI and XhoI digested pCMV-myc (Clontech). PCR using the 5'-terminal primer CCGCTCGAGCGGAATTCAAGCAGAAA and the 3' -terminal primer CGCGGATCCTCAGCTGTTGACTCACCAAA amplified the JX2 domain of human Nup358. The primer pair GCTCAGAATTCATGGCGGATCCAGCC and CAGATGGGCCCGAGAGACTGTATTCTTGATGGTCTTTG was used to amplify the coding sequence for the first 332 N-terminal amino acids of rat Kif5C. PCR products were ligated into pEGFP-N1 (Clontech) using the XhoI and BamHI or EcoRI and ApaI restriction sites, respectively. Cells grown on 12 mm glass coverslips were transfected with plasmid DNA using FuGENE 6 (Roche) according to the manufactures protocol. Alternatively, HeLa or HEK293T cells were transferred into a 4 mm gap Gene Pulser cuvette (Bio-Rad Laboratories) and transfected using the BTX T 820 electroporator (BTX Instrument Division, Harvard Apparatus, Holliston, MA USA).

Recombinant proteins, GST pull-downs and co-immune-precipitation

Glutathione-S-transferase (GST) fusion proteins of Klc2 and the TPR-domain of Klc2 were expressed in *Escherichia coli* strain BL21 pRep4 under standard conditions, and purified with glutathione-Sepharose 4B (Amersham Biosciences). Ad5 capsid protein hexon was recovered from top fractions of CsCl density gradients used for the purification of Ad particles (Greber et al., 1993) and purified on Mono-Q-anion exchange column (BioLogic, Bio-Rad Laboratories, Hercules, CA USA) as described before (Trotman et al., 2001). A purity of 95% was estimated by SDS-PAGE and Coomassie Blue staining. The preparation was free of detectable pIX, penton base and fiber, as concluded from Western blotting.

Purified GST, GST-TPR (15 µg) bound to glutathione-Sepharose 4B beads were incubated with 40 µg Ad2, Ad5, Ad5 delta pIX or Ad5 hexon in 1 ml cytosol buffer (25 mM Hepes, pH 7.0, 125 mM K-acetate, 2.5 mM Mg-acetate, 1 mM DTT, 0.5% Triton X-100 and protease inhibitors (1 mM phenylmethylsulfonyl fluoride and 1 µg each of chymostatin, leupeptin, aprotinin, and pepstatin) at 4°C for 1h. Vice versa, 20 µg of biotinylated Ad2 bound to streptavidin agarose (Sigma, Fluka, Switzerland) was incubated with soluble GST or GST-TPR of Klc2 in 1 ml cytosol buffer at 4°C for 1h. After washing the beads three times with cytosol buffer, bound proteins were eluted in SDS-PAGE loading buffer and analysed by Western blotting. HEK293T expressing HA-Klc1 and myc-pIX were lysed in IP lysis buffer (50 mM Tris-HCl pH7.4, 150 mM NaCl, 1 mM DTT, 1 mM EDTA, 1% NP40 supplemented with Protease arrest (G-Biosciences, Maryland Heights, MO) and Phosphatase inhibitor cocktail 2 (Sigma). Immune-precipitation was performed using rabbit anti-pIX antibodies. Precipitated proteins were separated on 8-16% poly-acrylamid gels (Pierce Biotechnology), transferred to Immobilon-P PVDF membranes (Millipore) and probed by the indicated antibodies.

Infection analyses by fluorescence microscopy

Infections of HeLa cells were carried out as described (Suomalainen et al., 1999; Trotman et al., 2001). Cells grown on 12 mm glass coverslips (Assistant) were treated with drugs for 20 min and incubated with 0.4 µg of Ad2-TR or Ad2-atto565 in cold RPMI medium (Gibco-BRL) supplemented with 0.2 mg/ml BSA for 60 min. Unbound virus was washed off and cells were incubated in DMEM containing 0.2 mg/ml BSA with or without drug at 37°C for indicated times. Cells were either subjected to live cell microscopy or fixed in 3% pFA for 20 min, quenched with 25 mM NH_4Cl in PBS for 5 min and permeabilized with 0.5% Triton X-100 in PBS for 5 min. Samples were processed for immune-fluorescence analysis using indicated antibodies and mounted in 3 µl mounting medium (DAKO, Carpinteria, CA, USA). HeLa cells were washed DMEM-BSA and incubated with 8000 viral particles per cell at 37°C for 1 h, washed with DMEM-BSA and incubated for 5 h (Ad5-GFP) or 8 h (Ad2-mRFP). Adenovirus-mediated expression of mRFP in GFP, GFP-TPR, p50-GFP, JX2-GFP and Kif5C (1-332)-GFP transfected HeLa cells was quantified from confocal laser scanning microscope images of fixed samples. After background subtraction, fluorescence intensities from all section of a confocal stack were summed up and quantified using ImageJ program (NIH).

Infection analyses by flow cytometry

Virus-mediated transduction of fluorescent proteins in RNAi silenced cells was analysed by flow cytometry using a Beckman FC500 cytometer equipped with a 488 nm Argon laser and a 638 nm solid-state laser. 10000 viable cells were counted per sample.

Electroporation, transfection and image analyses

Hela-K cells were electroporated with either pcDNA-mRFP1-N (3.9 µg) or pcDNA-mRFP1-N (3.9 µg) + pS-Nup358 (6.1 µg) (molar ratio = 1:3), seeded on a 10 cm

dish, detached with trypsin/EDTA 24 h later, diluted into growth medium, counted and placed into a 96-well plate at 0.1 ml / well containing 1000-2000 cells. Cells were incubated for 72h, and infected with Ad5-GFP for 1 h at 8000 particles per cell (multiplicity of infection moi 5, assuming that 3% of virus particles bind to the cells under these conditions), or with HSV-GFP in D-MEM/0.2%BSA at similar moi. Cells were incubated for 6 or 9 h, fixed with pFA, quenched by washing in 25mM NH4Cl, permeabilized with 0.5% Triton X-100 in PBS, stained with DAPI (4',6-diamidino-2-phenylindole), washed in PBS and imaged at the MDC-Imaging station using a 10x S Fluor objective (NA 0.5) and a Cool SNAP-HQ monochrome camera operated at 2x2 binning on a 1392x 1040 pixel array. 12-bit TIF images were analysed with custom programmed scripts using MATLAB software (MathWorks, Inc. Natick, MA, USA). Nuclei were detected in the DAPI images using the Otsu's thresholding method (Otsu, 1979), and the mean pixel intensities over the nuclear area extracted. Thresholds for both, transfected and infected cells were set manually based on untreated, uninfected and single transfected cells. The infection index of transfected cells was calculated as follows: RFP positive / (RFP positive plus double positive)*100.

Photo-conversion of Kaede-Nup214

DNA encoding the photo-convertible fluorescent protein Kaede (pKaede-S1, MBL International Corporation, Woburn, MA, USA, Ando et al., 2002) was cloned into the expression vector containing human Nup214 cDNA (kindly provided by M. Fornerod, Erasmus University Medical Center, Rotterdam, The Netherlands), and transfected into HeLa-K cells with JetPEI (Polyplus Transfection, Illkirch, France) on 12 mm glass coverslips for 48 h. Cells were mounted onto a home-made slide holder, overlaid with 0.5 ml live imaging medium (Hank's Buffered Salt Solution with 0.5% BSA and 1mg/ml ascorbic acid, pH 7.2-7.4), inoculated with 0.5 µg of Ad2-atto647, and photo-converted in 5 optical layers across the entire nucleus with a UV-laser at 355 nm in combination with a diode laser at 405 nm for 10 s on an

SP5 Leica confocal laser scanning microscope recording the X-Y position of the photo-converted cells. Infection continued until 90-160 min, and entire optical stacks from photo-converted cells were acquired at 488, 561 and 633 nm excitation to record non-converted Kaede-Nup214, converted Kaede-Nup214 and Ad2-atto647. Single sections were analysed for colocalization of converted Kaede-Nup214 and Ad2-atto647, and images were displayed after deconvolution by Huygens software (Scientific Volume Imaging, Hilversum, The Netherlands). The total number of Ad2-atto647 particles was analysed by maximum projections of image stacks and processing by a global threshold method (see supplemental data).

Image acquisition and quantification

Confocal images were recorded on a Leica SP2 confocal microscope (Heerbrugg, Switzerland) using 63x oil immersion objective, UV excitation at 351 and 364 nm, FITC 488 nm, TR 568 nm, Cy5 647 nm controlled by an accusto-optical beam splitter in sequential recording mode with 0.5 µm section distance. For time-lapse fluorescence microscopy of Ad2-atto565 infected HeLa cells we used a spinning disc confocal microscope based on an Olympus IX81 inverted microscope with an UPlanApo100x objective (Olympus Optical AG, Switzerland). Cells were imaged in an incubator box at 37°C (Live Imaging Services, Switzerland) in HBBS medium (Gibco-BRL) complemented with 0.5% BSA and 1 mg/ml ascorbate, pH7.2. Innova 70C mixed-gas laser (Coherent, Germany) was used for excitation at 488 and 568 nm, a Yokogawa scanning head QLC100 (VisiTech International, UK) with a triple band-pass dichroic mirror (488 nm/565 nm/647 nm, Chroma, USA), a Dualview MultiSpec-MicroImager (Optical Insights, USA) for simultaneous dual colour imaging and a cooled, back-illuminated, 16-bit monochrome CCD camera (Cascade 512, Roper Scientific, USA) for fluorescence image recording (Visitron, Puchheim, Germany). The microscope was controlled with the Metamorph software package (Universal Imaging, USA). Quantitative co-localization analyses

were performed as described before (Trotman et al., 2001). Electron microscopy and Ad2 particle quantification in subcellular regions were carried out as described (Nakano et al., 2000). Further information about image quantifications are described in the Suppl. Methods.

Quantification of subcellular virus localization

Ad2-TR infected cells were fixed and 12-bit CLSM images sequentially recorded with 0.5 µm distance between sections. Using the Sobel edge detector algorithm the cell shape was identified in differential interference contrast (DIC) images (Sobel and Feldman, 1968). Cell nuclei were detected on DAPI images by global thresholding. Peripheral regions of the cells were defined as a band with a width of 3.5 µm at the periphery of the binarized cell shape images. Similarly, the nuclear rim was defined as a band extending 1.3 µm to the cytoplasm and 1.3 µm into the nucleus whereas the nuclear area was defined as the area inside the nuclear rim band. The cytoplasmic area was defined as the area between nuclear rim and peripheral region. Virus fluorescence images were background subtracted and low pass-filtered to improve the signal to noise ratio. The signals in all defined regions were calculated for each section of the CLSM image stack by adding the pixel intensities. Nuclear virus was plotted as the mean intensities of nuclear rim and nuclear region. Results were expressed as mean values of indicated samples (n) including SEM.

Quantification of co-localization

Relative co-localization of Ad2-TR with GFP-TPR or GFP-Nups were scored on single-section CLSM images of an Ad2-TR infection time course. A threshold was subtracted from all three sequentially recorded channels (green: GFP-TPR/GFP-Nup, red: Ad2-TR, Cy5: disassembled hexon) and the area of overlapping signals was determined using the NIH ImageJ colocalization plug-in. The area of

apparently intact particles colocalizing with GFP-TPR (double positive for Ad2-TR and GFP-TPR, hexon-negative) was determined by subtracting the area of disassembled particles colocalizing with GFP-TPR (triple positive for Ad2-TR, GFP-TPR and hexon) from the total area of Ad2-TR colocalization with GFP-TPR (Ad2-TR and GFP-TPR positive). The results were normalized to the total area of Ad2-TR within a cell and expressed as mean values of the indicated number of analysed cells (n) including standard error of the mean.

Virus disassembly by indirect immune-fluorescence

Virus uncoating was measured by indirect immune-fluorescence with a conformation sensitive rabbit anti-hexon R70 provided by M. Horwitz (Albert Einstein College of Medicine, New York), as described (Trotman et al., 2001). After background subtraction from single section confocal images, stacks were projected and fluorescence intensities summed up. The fluorescence intensities of disassembled particles were measured within the cellular area outlined on DIC images.

GFP-pV dissociation from Ad2-atto647

GFP and atto-fluorescence were recorded with the automated ImageXpress^{MICRO} fluorescence microscope (Molecular Devices) using a Nikon 40x air objective NA 0.95, Semrock BrightLine filters (GFP-3035B-NTE-ZERO, Cy5-4040A-NTE-ZERO and DAPI-5060B-NTE-ZERO) and the Molecular Devices MetaXpress 2 software, as described (Puntener et al., 2011). Nine individual regions per well were recorded as stacks comprised of 9 sections with a z-distance of 1 µm and images were saved as 16 bit TIFFs. Illumination times were 6 seconds for GFP, 8 seconds for atto647 and 5 ms for DAPI without binning. Recorded images were processed as follows. To correct for uneven illumination across the field of view, a well containing no cells was recorded using identical settings (background stack). From

each slice in the sample stack the pixel intensity of the corresponding slice in the background stack was subtracted. Chromatic aberrations caused a shift of the virus position in the GFP channel relative to its position in the atto647 channel. This was corrected with a custom written Matlab script. The pixel intensity value associated with each element in the image matrix was distributed into elements of a new matrix relative to the calculated shift. This resulted in a new image matrix where intensity values were shifted to the corrected image locations.

An algorithm programmed in MatLab was used for particle scoring. In brief, Otsu's method (Otsu, 1979) was used for thresholding of maximum intensity projections generated from background and aberration corrected images acquired in the atto647 channel. A manually set area threshold was used to attribute contiguous pixel over the grey threshold to virus particles in an image mask. This image mask was subsequently employed to measure average fluorescent intensities over the particle areas in both average intensity projections from GFP channel images and atto647 channel images. Particle size, average GFP fluorescence intensity, average atto647 fluorescence intensity, and the ratio (GFP/atto647) of the two aforementioned intensities were extracted. Average GFP/atto647 intensities were plotted against time, including SEM. P-values were obtained by students t-test.

Spinning disc confocal microscopy

The set up included a Olympus IX81 inverted microscope (Olympus Optical AG, Switzerland), a Yokogawa scanning head QLC100 (VisiTech international, UK) with a triple band-pass dichroic mirror (Chroma, USA), a Dualview MultiSpec-MicroImager (Optical Insights, USA) for simultaneous dual color imaging, and a cooled, back-illuminated, 16-bit monochrome CCD camera (Cascade 512, Roper Scientific, USA) controlled by Metamorph software (Universal Imaging, USA).

Purification and microinjection of dextrans

Fluorescently labeled 2000 kDa dextran-TMR (tetra-methyl-rhodamine) and 500 kDa dextran-FITC (fluorescein-iso-thio-cyanate) were fractionated on Superose 6-HR 10/30 column (Pharmacia, Sweden) using Bio-Rad Biologic System. The column was equilibrated in microinjection buffer (0.12 M KCl, 0.01 M Tris-HCl, pH 7.4), samples were applied using a 100 µl sample loop, and 96 x 0.3 ml fractions were collected at 0.3 ml/min flow rate. Analyses of fractions were carried out in a Safire-2 microplate fluorescence reader. The exclusion limit of Superose 6-HR is 40'000 kDa for globular proteins (7.5 ml elution volume). Fractions 27-32 (elution volume 8.1-9.6 ml) from the 2000 kDa dextran-TMR were pooled and their homogeneity confirmed by reanalysis on on Superose 6-HR 10/30 (see Fig. 6d). Dextrans are known to have a larger Stokes radius than globular proteins (Armstrong et al., 2004), for example, 500 kDa dextran has a Stokes radius of 26.9 nm, whereas thyroglobulin (MW 669'000) has one of 8.6 nm. For the 500 kDa dextran-FITC, fractions 44-49 (13.2-14.7 ml) were pooled (Fig. 6d). These fractions had a slightly slower elution time than the peak of the 500 kDa dextran-FITC (12-12.6 ml, not shown), and were likely smaller than 500 kDa. They were, however, larger than the 40 kDa dextran-FITC, the peak of which eluted at 16.2-17.7 ml (Fig. 6d). The 40 kDa dextran-FITC had a broad distribution profile, which largely overlapped with the fractions 44-49 from the 500 kDa dextran-FITC, but did not overlap with fractions 27-32 from 2000 kDa dextran-TMR. Fractions 27-32 of 2000 kDa dextran-TMR, and 44-49 of 500 kDa dextran-FITC were concentrated by ultrafiltration (Amicon Ultra-4 10K, Millipore) and microinjected at concentrations of 0.1 to 0.5 mg/ml as described (Nakano and Greber, 2000). Alternatively, non-fractionated, broad range 40 kDa dextran-FITC was injected, and cells were inoculated with 10^3 Ad2-atto565 particles per cell for 30 min (moi 50). The ratio between the average fluorescence outside the nuclear rim and a spot inside the nucleus was measured, and represented as cytoplasmic / nuclear ratio. T-tests were done with two-tailed distributions, and two samples unequal variance.

Data representation

Figures were constructed using Adobe Photoshop and Illustrator. Graphs represent mean values of analysed samples (n) including the SEM, and p-values from t-tests.

Supplemental References

Ando, R., Hama, H., Yamamoto-Hino, M., Mizuno, H., and Miyawaki, A. (2002). An optical marker based on the UV-induced green-to-red photoconversion of a fluorescent protein. Proc Natl Acad Sci U S A *99*, 12651-12656.

Armstrong, J.K., Wenby, R.B., Meiselman, H.J., and Fisher, T.C. (2004). The hydrodynamic radii of macromolecules and their effect on red blood cell aggregation. Biophysical journal *87*, 4259-4270.

Bernad, R., van der Velde, H., Fornerod, M., and Pickersgill, H. (2004). Nup358/RanBP2 attaches to the nuclear pore complex via association with Nup88 and Nup214/CAN and plays a supporting role in CRM1-mediated nuclear protein export. Mol Cell Biol *24*, 2373-2384.

Bodoor, K., Shaikh, S., Salina, D., Raharjo, W.H., Bastos, R., Lohka, M., and Burke, B. (1999). Sequential recruitment of NPC proteins to the nuclear periphery at the end of mitosis. J Cell Sci *112 (Pt 13)*, 2253-2264.

Burkhardt, J.K., Echeverri, C.J., Nilsson, T., and Vallee, R.B. (1997). Overexpression of the dynamitin (p50) subunit of the dynactin complex disrupts dynein-dependent maintenance of membrane organelle distribution. J Cell Biol *139*, 469-484.

Cai, Y., Singh, B.B., Aslanukov, A., Zhao, H., and Ferreira, P.A. (2001). The docking of kinesins, KIF5B and KIF5C, to Ran-binding protein 2 (RanBP2) is mediated via a novel RanBP2 domain. J Biol Chem *276*, 41594-41602.

Fornerod, M., van Deursen, J., van Baal, S., Reynolds, A., Davis, D., Murti, K.G., Fransen, J., and Grosveld, G. (1997). The human homologue of yeast CRM1 is in a dynamic subcomplex with CAN/Nup214 and a novel nuclear pore component Nup88. Embo J *16*, 807-816.

Giepmans, B.N., Adams, S.R., Ellisman, M.H., and Tsien, R.Y. (2006). The fluorescent toolbox for assessing protein location and function. Science *312*, 217-224.

Greber, U.F., Willetts, M., Webster, P., and Helenius, A. (1993). Stepwise dismantling of adenovirus 2 during entry into cells. Cell *75*, 477-486.

Hutten, S., Flotho, A., Melchior, F., and Kehlenbach, R.H. (2008). The Nup358-RanGAP Complex Is Required for Efficient Importin {alpha}/{beta}-dependent Nuclear Import. Mol Biol Cell *19*, 2300-2310.

Imelli, N., Ruzsics, Z., Puntener, D., Gastaldelli, M., and Greber, U.F. (2009). Genetic reconstitution of the human adenovirus type 2 temperature-sensitive 1 mutant defective in endosomal escape. Virol J *6*, 174.

Nakano, M.Y., Boucke, K., Suomalainen, M., Stidwill, R.P., and Greber, U.F. (2000). The first step of adenovirus type 2 disassembly occurs at the cell surface, independently of endocytosis and escape to the cytosol. J Virol *74*, 7085-7095.

Nakano, M.Y., and Greber, U.F. (2000). Quantitative microscopy of fluorescent adenovirus entry. J Struct Biol *129*, 57-68.

Newsome, T.P., Scaplehorn, N., and Way, M. (2004). SRC mediates a switch from microtubule- to actin-based motility of vaccinia virus. Science *306*, 124-129.

Otsu, N. (1979). A threshold selection method from gray-level histograms 9: 62–66. IEEE Transactions on Systems, Man and Cybernetics *9*, 62-66.

Pfister, K.K., Wagner, M.C., Stenoien, D.L., Brady, S.T., and Bloom, G.S. (1989). Monoclonal antibodies to kinesin heavy and light chains stain vesicle-like structures, but not microtubules, in cultured cells. J Cell Biol *108*, 1453-1463.

Puntener, D., Engelke, M.F., Ruzsics, Z., Strunze, S., Wilhelm, C., and Greber, U.F. (2011). Stepwise loss of fluorescent core protein V from human adenovirus during entry into cells. J Virol *85*, 481-496.

Rosa-Calatrava, M., Grave, L., Puvion-Dutilleul, F., Chatton, B., and Kedinger, C. (2001). Functional analysis of adenovirus protein IX identifies domains involved in capsid stability, transcriptional activity, and nuclear reorganization. Journal of Virology *75*, 7131-7141.

Russell, W.C., Valentine, R.C., and Pereira, H.G. (1967). The effect of heat on the anatomy of the adenovirus. J Gen Virol *1*, 509-522.

Sobel, I., and Feldman, G. (1968). A 3x3 Isotropic Gradient Operator for Image Processing, Vol 73 (New York, John Wiley & Sons, Ltd).

Suomalainen, M., Nakano, M.Y., Boucke, K., Keller, S., Stidwill, R.P., and Greber, U.F. (1999). Microtubule-dependent minus and plus end-directed motilities are competing processes for nuclear targeting of adenovirus. J Cell Biol *144*, 657-672.

Trotman, L.C., Mosberger, N., Fornerod, M., Stidwill, R.P., and Greber, U.F. (2001). Import of adenovirus DNA involves the nuclear pore complex receptor CAN/Nup214 and histone H1. Nature Cell Biology *3*, 1092-1100.

Vellinga, J., Van der Heijdt, S., and Hoeben, R.C. (2005). The adenovirus capsid: major progress in minor proteins. J Gen Virol *86*, 1581-1588.